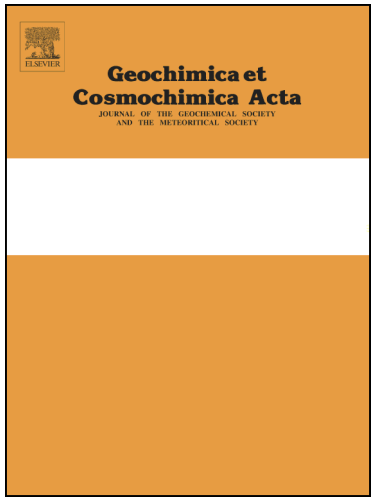

Preservation of an Archaean whole rock Re-Os isochron for the Venetia lithospheric mantle: evidence for rapid crustal recycling and lithosphere stabilisation at 3.3 Ga

Quinten H.A. van der Meer, Martijn Klaver, Laurie Reisberg, Amy J.V. Riches, Gareth R. Davies

PII: S0016-7037(17)30277-6
DOI: http://dx.doi.org/10.1016/j.gca.2017.05.004
Reference: GCA 10271

To appear in: *Geochimica et Cosmochimica Acta*

Received Date: 1 December 2016
Revised Date: 2 May 2017
Accepted Date: 4 May 2017

Please cite this article as: van der Meer, Q.H.A., Klaver, M., Reisberg, L., Riches, A.J.V., Davies, G.R., Preservation of an Archaean whole rock Re-Os isochron for the Venetia lithospheric mantle: evidence for rapid crustal recycling and lithosphere stabilisation at 3.3 Ga, *Geochimica et Cosmochimica Acta* (2017), doi: http://dx.doi.org/10.1016/j.gca.2017.05.004

Preservation of an Archaean whole rock Re-Os isochron for the Venetia lithospheric mantle: evidence for rapid crustal recycling and lithosphere stabilisation at 3.3 Ga

Quinten H.A. van der Meer*[+1,3], Martijn Klaver[+1,2], Laurie Reisberg[4], Amy J.V. Riches[5], Gareth R. Davies[1]

[1] Department of Geology and Geochemistry, Vrije Universiteit Amsterdam, De Boelelaan 1085, 1081HV Amsterdam, The Netherlands

[2] School of Earth Sciences, University of Bristol, Wills Memorial building, Queen's Road, Bristol BS8 1RJ, United Kingdom

[3] Department of Geological Sciences, 13 University Avenue, University of Cape Town, Rondebosch 7701, South Africa

[4] Centre de Recherches Pétrographiques et Géochimiques, UMR 7358 CNRS-Université de Lorraine, Vandoeuvre-lès-Nancy 54500, France

[5] Department of Earth Sciences, University of Durham, Durham, DH1 3LE, United Kingdom.

[+]Authors made equal contributions

*Corresponding author: *qvandermeer@gmail.com*

ABSTRACT

Re-Os and platinum group element analyses are reported for peridotite xenoliths from the 533 Ma Venetia kimberlite cluster situated in the Limpopo Mobile Belt, the Neoarchaean collision zone between the Kaapvaal and Zimbabwe Cratons. The Venetian xenoliths provide a rare opportunity to examine the state of the cratonic lithosphere prior to major regional metasomatic disturbance of Re-Os systematics throughout the Phanerozoic. The 32 studied xenoliths record Si-enrichment that is characteristic of the Kaapvaal lithospheric mantle and can be subdivided into five groups based on Re-Os analyses. The most pristine group I samples (n = 13) display an approximately isochronous relationship and fall on a 3.28 ± 0.17 Ga (95% conf. int.) reference line that is based on their mean T_{MA} age. This age overlaps with the formation age of the Limpopo crust at 3.35-3.28 Ga. The group I samples derive from ~50 to ~170 km depth, suggesting coeval melt depletion of the majority of the Venetia lithospheric mantle column. Group II and III samples have elevated Re/Os due to Re addition during kimberlite magmatism. Group II has otherwise undergone a similar evolution as the group I samples with overlapping $^{187}Os/^{188}Os$ at eruption age: $^{187}Os/^{188}Os_{EA}$, while group III samples have low Os concentrations, unradiogenic $^{187}Os/^{188}Os_{EA}$ and were effectively Re-free prior to kimberlite magmatism. The other sample groups (IV and V) have disturbed Re-Os systematics and provide no reliable age information. A strong positive correlation is recorded between Os and Re concentrations for group I samples, which is extended to groups II and III after correction for kimberlite addition. This positive correlation precludes a single stage melt depletion history and indicates coupled remobilisation of Re and Os. The combination of Re-Os mobility, preservation of the isochronous relationship, correlation of $^{187}Os/^{188}Os$ with degree of melt depletion and lack of radiogenic Os addition puts tight constraints on the formation and subsequent evolution of Venetia lithosphere. First, melt depletion and remobilisation of Re and Os must have occurred within error of the 3.28 Ga mean T_{MA} age. Second, the refractory peridotites contain significant Re despite recording >40 % melt extraction. Third,

assuming that Si-enrichment and Re-Os mobility in the Venetia lithospheric mantle were linked, this process must have occurred within ~100 Myr of initial melt depletion in order to preserve the isochronous relationship. Based on the regional geological evolution, we propose a rapid recycling model with initial melt depletion at ~3.35 Ga to form a tholeiitic mafic crust that is recycled at ~3.28 Ga, resulting in the intrusion of a TTG suite and Si-enrichment of the lithospheric mantle. The non-zero primary Re contents of the Venetia xenoliths imply that T_{RD} model ages significantly underestimate the true depletion age even for highly depleted peridotites. The overlap of the ~2.6 Ga T_{RD} ages with the time of the Kaapvaal-Limpopo collision is purely fortuitous and has no geological significance. Hence, this study underlines the importance of scrutiny if age information is to be derived from whole rock Re-Os analyses.

Keywords: *Re-Os chronology of peridotites; platinum group elements; Limpopo Mobile Belt; Kaapvaal Craton formation; melt extraction and metasomatism*

1. Introduction

The Re-Os isotope system has proven to be a powerful tool for constraining the timing of the formation of sub-continental lithospheric mantle (SCLM). During mantle melting, Re partitions into the melt whereas Os is highly compatible, thus allowing the use of model ages to date melt extraction events (Walker et al., 1989; Pearson et al., 1995). The high Os contents and very low Re/Os of refractory lithospheric mantle compared to melts, fluids and the continental crust imply that the SCLM Os-isotope compositions should be relatively resistant to modification. Despite the general robustness of the Re-Os system, complex multi-stage metasomatic processes have often modified or erased primary Os-isotope signatures of the SCLM (e.g., Griffin et al., 2004; Pearson et al., 2004; Luguet et al., 2015). The principal causes for disturbance include re-introduction of Re and/or radiogenic Os during metasomatism, sulphide mobility, interaction of xenoliths with their basaltic or kimberlitic host magmas and/or disproportional Os and Re loss during weathering (e.g. Handler et al., 1999; Pearson et al., 2004; Reisberg et al., 2004; Simon et al., 2007; Rudnick and Walker, 2009). In addition to the complexities caused by such disturbances, it is unclear whether the original melt extraction events would have left an isotopically homogeneous residue. For these reasons, convincing whole rock Re-Os isochronous relationships have not been found in peridotite xenolith suites (Aulbach et al., 2016), with the possible exception of a Proterozoic age recorded by peridotite xenoliths from the North China Craton (Gao et al., 2002). Nevertheless, Os model ages obtained from individual xenoliths (Walker et al., 1989) have been used extensively to obtain information on the timing of lithospheric melting episodes (e.g. Pearson and Wittig 2014).

To improve the temporal constraints on the formation and modification of the Kaapvaal SCLM, a suite of peridotite mantle xenoliths from the Venetia kimberlite mine, South Africa, were analysed for Re-Os isotope compositions and platinum-group-element (PGE; including Os, Ir, Ru, Pt and Pd) contents. These samples were previously characterised in van der Meer et al. (2013) and are obtained from relatively deep mining levels and drilled core. They therefore have suffered less from near-surface weathering than the Venetian peridotites analysed by Stiefenhofer et al. (1999) and Carlson et al. (1999). The 533 ± 4 Ma Venetia kimberlite cluster (Rb-

Sr isochron age; Allsop et al., 1995) is one of the oldest in the region and hosts refractory peridotite xenoliths that record up to 50 % melt depletion and represent a virtually complete section of the SCLM from 55 km to >170 km depth (Carlson et al., 1999; Stiefenhofer et al., 1999; Hin et al., 2009; van der Meer et al., 2013). As a result of the Cambrian kimberlite emplacement age, Venetia mantle xenoliths record the state of the SCLM prior to disturbance of the Re-Os isotope system and PGE systematics by pervasive metasomatic events imprinted in the lithospheric mantle throughout the region during the Mesozoic (e.g., Pearson et al., 1995; Carlson et al., 1999; Simon et al., 2007). Hence, these xenoliths have the potential to yield more reliable Re-Os age information than other Kaapvaal kimberlite-hosted peridotite suites.

We find that a subset of the studied samples, spanning nearly the entire depth range, displays coherent Re-Os systematics that show an approximately isochronous relationship. An important observation is that although Re contents are lower than those of fertile mantle (e.g. Becker et al., 2006; Aulbach et al., 2016), the Venetia xenoliths record time-integrated Re/Os values that are in excess of that expected for residues of >40 % melt depletion. This contradicts the generally accepted view that Re contents of highly depleted Archaean SCLM can be regarded as negligible prior to kimberlite emplacement (e.g., Pearson and Wittig, 2008; Rudnick and Walker, 2009; Pearson and Wittig, 2014; Aulbach et al., 2016) and has important implications for the accuracy of Re-depletion model ages (T_{RD}; Walker et al., 1989; Pearson et al., 1995).

2. Geological setting and petrography of the Venetia peridotite suite

The ~533 Ma Venetia kimberlite cluster (Allsopp et al., 1995) is situated in the Central Zone of the Limpopo Mobile Belt (LMB) in southern Africa (Fig. 1), and is underlain by thick SCLM (~220 km) as indicated by mantle tomography (James et al., 2001). Stabilisation of the crust of the LMB Central Zone occurred at 3.35-3.27 Ga. In contrast, amalgamation of the Kaapvaal and Zimbabwe Cratons to form the nucleus of the Kalahari Craton was achieved at 2.7-2.6 Ga (e.g., Millonig et al., 2008; Zeh et al., 2010; Khoza et al., 2013; Xie et al., 2017). The LMB Central Zone is believed to represent a separate micro-continent that was sandwiched between the Kaapvaal and Zimbabwe Cratons during their collision at 2.6-2.7 Ga, or accreted to either craton prior to that. Van der Meer et al. (2013) argued that refractory harzburgites and clinopyroxene-poor lherzolites from the SCLM beneath the Central Zone are indistinguishable from those of the Si-rich Kaapvaal Craton in terms of major elements, thus lending support to a prolonged joined history. In this scenario, the Central Zone could be viewed as one of the Kaapvaal terranes such as the adjacent Pietersberg Terrane, which is similar in size and orientation (Fig 1.), with the distinction that deeper crustal levels are exposed in the LMB. Previous studies of the Venetia xenolith suite by Stiefenhofer et al. (1999), Hin et al. (2009) and van der Meer et al. (2013) report ranges in olivine Mg# (molar Mg/[Mg+Fe]) of 89 to 94 with an average of 92.7 that corresponds to ~40 % melt depletion (Bernstein et al., 2007). The low-temperature (<1000 °C) xenolith suite displays Si-enrichment, demonstrated by modal orthopyroxene contents that are too high for the degree of melt depletion (e.g., Boyd, 1989). Metasomatic enrichment is also recognized in Venetian diamond inclusions (Aulbach et al., 2002; Richardson and Shirey, 2008; Richardson et al., 2009). In these aspects, the Venetia suite is indistinguishable from typical Kaapvaal SCLM (van der Meer et al., 2013). The main difference is that the Venetia xenolith suite

lacks the intense modal and cryptic melt metasomatism recognized in the majority of Kaapvaal SCLM samples that are hosted in younger kimberlites. Melt metasomatism in Kaapvaal peridotites is commonly attributed to metasomatism related to kimberlite magmatism from 120 to 90 Ma, and the eruption of the Karoo flood basalts at ~180 Ma (e.g., Grégoire et al., 2003; Simon et al., 2003, 2007; Kobussen et al., 2009; Giuliani et al., 2014). Critically, emplacement of the Venetia kimberlite predates these events. Silicate Fe-Ti-rich melt-related metasomatism is only recognized in Venetian high-temperature lherzolites that are derived from the lower parts of the Venetia SCLM (Barton and Gerya, 2003; Hin et al., 2009; van der Meer et al., 2013).

Peridotite xenoliths hosted in the Venetia kimberlite were divided into three groups by van der Meer et al. (2013). The low-temperature, equant coarse crystalline lherzolites (Low-T lherzolites) are derived from 50-130 km depth and contain an equilibrium mineral assemblage of olivine, orthopyroxene, clinopyroxene ± garnet ± spinel. The latter three phases occur as lobate, irregular intergrowths in association with orthopyroxene. Geochemical and petrographic evidence indicates that garnet and clinopyroxene formed through exsolution from aluminous high-temperature orthopyroxene and were not directly introduced by melt metasomatism (Hin et al., 2009; van der Meer et al., 2013). Prior to exsolution, the Low-T lherzolites were clinopyroxene-free harzburgites, in accordance with the high degrees of melt depletion suggested by their major element chemistry (van der Meer et al., 2013). The high-temperature (>1000 °C) xenolith suite comprises equant coarse harzburgites (High-T harzburgites) that are transitional to porphyroclastic lherzolites (High-T lherzolites). Both High-T groups derive from 130 km to 235 km depth and appear to be intermixed in the lower SCLM. Modal olivine contents increase from the Low-T lherzolites to the High-T lherzolites; the High-T harzburgites are intermediate between the two. The High-T harzburgites contain no primary clinopyroxene or spinel and garnet forms rounded grains ranging in size from 4 mm to 10 mm, which contrasts with smaller, lobate garnet in the Low-T lherzolites. In the High-T lherzolites, coarse (up to 1 cm) round garnet, smaller orthopyroxene and clinopyroxene crystals are set in a fine-grained olivine matrix. Olivine Mg# is significantly lower in the High-T lherzolites (average 91.5) than in the other two groups and, in combination with higher whole rock TiO_2 contents, suggests metasomatism by 1-5 % of the host kimberlite or a related magma prior to eruption (Hin et al., 2009; van der Meer et al., 2013). Interaction of the High-T suite with asthenosphere-derived melts is consistent with an inflection of the geothermal gradient, driving the samples off the cratonic “steady-state geotherm” (based on Low-T peridotites and non-touching diamond inclusion pairs; van der Meer et al., 2013) to temperatures that are elevated by >200 °C. Based on this evidence, infiltration of (proto)kimberlitic melts is considered to have caused localised heating of the lower lithosphere and metasomatism of the High-T lherzolites, but left very few metasomatic effects on the Low-T suite and most High-T harzburgites (van der Meer et al., 2013). In addition to the peridotites, rare pyroxenites, ranging from garnet-clinopyroxenites to olivine websterites, and a single eclogite have also been reported in Venetia (Stiefenhofer et al., 1999; Hin et al., 2009; van der Meer et al., 2013).

3. Analytical techniques

Rhenium-osmium analyses of 25 Venetia mantle xenolith samples were carried out at CRPG-CNRS in Nancy, France. Detailed petrographic descriptions, whole rock and mineral major element data for the studied samples are given in van der Meer et al. (2013). For Re-Os isotope analysis, 1 gram of whole rock powder spiked with ^{185}Re and ^{190}Os was digested in 6.5 ml reverse aqua regia in a high-pressure asher (Anton Paar HPA-S; Reisberg and Meisel, 2002). Osmium was separated from the matrix by bromine liquid-liquid extraction and subsequently purified through micro-distillation (Birck et al., 1997). The osmium fractions were loaded onto Pt filaments together with a $Ba(OH)_2$ activator and measured as OsO_3^- by N-TIMS (Creaser et al., 1991; Völkening et al., 1991) on a Finnigan MAT 262 TIMS in static multi-collection mode. Mass 233 ($^{185}ReO_3$) was monitored throughout the run to assure that potential isobaric interferences from $^{187}ReO_3$ were insignificant. Data were processed offline to correct for spike contributions, ^{17}O and ^{18}O oxide interferences and mass fractionation assuming a $^{192}Os/^{188}Os$ normalizing ratio of 3.08271. Rhenium was separated by anion exchange chemistry and measured on an Elan 6000 ICP-MS. Rhenium concentrations were corrected for an average total procedural blank of 3.6 pg; osmium blanks were <200 fg and considered negligible (generally <0.02%). The LOST Os-standard yielded an average $^{187}Os/^{188}Os$ of 0.10695 ± 0.00025 (2 SD; n=17) in agreement with the accepted value for this standard (0.106916 ± 0.000010). Replicate analyses of peridotite reference material UB-N yield average values of 0.1274 ± 0.0008 for $^{187}Os/^{188}Os$, 3.56 ± 0.25 ppb Os, and 0.211 ± 0.013 ppb Re (2 SD; n=3), in agreement with published values (Meisel et al., 2003).

Abundances of PGEs and replicate Os isotope analyses were determined at the University of Durham, UK, using ~1 g of powder from the same batch used in Nancy. A ^{190}Os–^{191}Ir–^{99}Ru–^{194}Pt–^{106}Pd–^{185}Re mixed spike was added to the powders prior to digestion in inverse-aqua regia at high-pressure and high-temperature (~300°C, 18 hours) in quartz vessels enclosed in a high pressure asher. Sample processing followed the protocols detailed by Dale et al. (2012) and Ishikawa et al. (2014). To ensure efficient extraction of PGEs, particularly Re and Ru, a desilicification treatment was applied to the residual solids after aqua regia digestion. Chemical separation employed an anion exchange chromatography routine modified after Pearson and Woodland (2000). Abundances of PGE (Ir, Ru, Pt and Pd) and Re were determined by inductively-coupled plasma mass spectrometry using a ThermoFinnigan Element 2 at the University of Durham in the Durham Geochemistry Centre. Standard (Hf, Zr, Y, and Mo) solutions (all 1 ppb) were analysed at the start, middle and end of each session to quantify the degree of mass fractionation and the production rates of positively charged Hf, Zr, Y, and Mo-oxides (all <0.8%), which have equivalent masses to isotopes of Ir, Pt, and Pd. Os isotope were measurement by N-TIMS using similar operational procedures to those in Nancy, but using a ThermoFinnigan Triton at the Durham Geochemistry Centre. All Os-isotope beams and mass 233, corresponding to $^{185}ReO_3^-$ but also other molecular interferences, were measured sequentially using an axial secondary electron multiplier. Each isotope mass was centred at the start of the analysis. Eighty ratios were collected during each set of analyses made via peak hopping and integration times ranged between 1.05 and 8.39 seconds depending on the beam intensity. All raw Os-isotope data were exported and re-processed offline to apply an O-isotope

interference correction, followed by an iterative mass fractionation correction and correction for the spike composition and $^{187}ReO_3^-$ interference. The $^{187}ReO_3/^{188}OsO_3$ ratios determined during all Os-isotope measurements of the studied peridotite samples were ≤0.0004. All Os-isotope ratios, including $^{187}Os/^{188}Os$, were mass fractionation corrected using a $^{192}Os/^{188}Os$ ratio of 3.08271 and an exponential law.

Peridotite reference material GP-13 was processed with the samples analysed in Durham and is reported in Tables 1 and 2 along with previously published values. At Durham, blank concentrations applied to the samples are, with a few exceptions, <8 % for Re, Ir, Pt, Pd, and Ru, <5% for Re and <1 % for Os-abundances. For corrections, the blank is assumed to have $^{187}Os/^{188}Os$ of 0.32; the average of two measured blanks in this session. The average composition of DROsS measured on 100 pg and 10 pg loads during the period of analyses at Durham is 0.160518 ± 0.00057 (2SD, *n* = 4) and is within uncertainty of the in-house long-term value for measurement using Faraday cup and SEM protocols (0.16078 ± 0.00168 2SD, *n*= 458, and in agreement with that reported by Nanne et al., 2017).

Duplicate analyses for ATC 720 and ATC 722 at Nancy yielded almost identical results. Measurements of the same samples between different labs however, are outside analytical error but the difference is comparable to the reproducibility of three separate analyses of AT 1333 run at Durham (Table 1). The $^{187}Os/^{188}Os$ isotopic compositions of the two procedural blanks determined using the peridotite-specific quartz asher vessels and reagents dedicated to PGE-processing at Durham differed from one another. The blank-corrected isotopic compositions of the samples are sensitive to the blank composition assumed during offline processing (laboratory ID # P248-6; 7.23 pg of Os and a $^{187}Os/^{188}Os$ = 0.45 ± 0.01 and laboratory ID # P249-1; 2.48 pg of Os and a $^{187}Os/^{188}Os$ = 0.194 ± 0.004). We used an average value based on the two measured blanks, if we were to apply only the second of these (P249-1), the agreement between the measured $^{187}Os/^{188}Os$ of a greater number of the samples measured at both Durham and Nancy improves and will generally be within uncertainty of one another. Osmium isotope data obtained in Nancy are reported and discussed throughout the manuscript.

Osmium model ages (T_{RD} and T_{MA}) are calculated following Shirey and Walker (1998) using a mantle evolution curve based on ordinary chondrites, with $^{187}Os/^{188}Os$ = 0.1283 and $^{187}Re/^{188}Os$ = 0.422 (Walker et al., 2002) and a ^{187}Re decay constant of 1.666×10^{-11} yr^{-1} (Smoliar et al., 1996). Rhenium-depletion ages (T_{RD}) and $^{187}Os/^{188}Os$ at the time of eruption ($^{187}Os/^{188}Os_{EA}$) employ a kimberlite emplacement age of 533 Ma for the Venetia kimberlite cluster (Allsopp et al., 1995). We note that T_{MA} values are obtained by extrapolating $^{187}Os/^{188}Os$ values back in time using the measured $^{187}Re/^{188}Os$ until intersection with the mantle evolution curve. They should therefore in theory reflect the actual age of melt extraction. This formulation is, however, sensitive to disturbance of Re/Os. In contrast, T_{RD} ages calculate the intersection of $^{187}Os/^{188}Os_{EA}$ with a model reservoir assuming total absence of Re, i.e. without radiogenic ingrowth prior to kimberlite eruption. T_{RD} ages can be disrupted by mobility of Os but are not affected by perturbation of Re/Os during emplacement and must always be viewed as minimum values.

4. Results

The Re-Os dataset for the Venetia xenolith suite, including seven samples previously reported by Carlson et al. (1999), is listed in Table 1. Re-Os systematics of the Venetia suite are similar to those of Kaapvaal and other kimberlite-hosted SCLM samples. Most samples are depleted in Re compared to estimates for primitive upper mantle (PUM; 0.4 ppb; Becker et al., 2006) and Archean convecting mantle (ACM; 0.27 ppb; Aulbach et al., 2016), consistent with their refractory nature. Approximately a third of the samples show elevated Re/Os (>0.04), possibly as a result of kimberlite infiltration (Fig. 2a). Osmium contents vary from 11.3 ppb in a High-T lherzolite down to ~100 ppt in a High-T harzburgite, with the majority of the samples having between 2 and 5 ppb Os. The median Os abundance is 3.8 ppb, within the range of concentrations typically observed in kimberlite-hosted peridotites (Maier et al., 2012), similar to the PUM (3.9 ppb; Becker et al., 2006) and ACM (3.4 ppb; Aulbach et al., 2016) values. Peridotite samples yield $^{187}Os/^{188}Os$ from 0.106 to 0.124 (Fig. 3) and T_{RD} ages predominantly > 2.5 Ga, thus confirming the conclusion by Carlson et al. (1999) that the mantle beneath the LMB is Archaean in age (Table 1). Olivine websterite sample ATC 727 has $^{187}Re/^{188}Os$ and $^{187}Os/^{188}Os$ values within the range of the Venetia peridotites, but garnet clinopyroxenite AT 1198 is distinct. This pyroxenite has moderately high Re content (409 ppt), but a very low Os content (56 ppt) and associated radiogenic $^{187}Os/^{188}Os$ of 2.07, corresponding to a model age (T_{MA}) of 2.62 Ga. On the basis of its high Re/Os and distinct major element composition (e.g., 8.2 wt. % Al_2O_3; van der Meer et al., 2013), AT 1198 does not appear to be a refractory peridotite, but more likely an ultramafic cumulate.

Platinum Group Element concentrations for a selection of samples are reported in Table 2. Concentrations of I-PGE (Os, Ir, Ru) are similar to or higher than PUM values and PUM normalised concentration patterns are relatively flat. ATC 725 differs from other studied samples in having significantly lower IPGE (Os, Ir, Ru) abundances. Concentrations of P-PGE (Pd and Pt) and Re are sub-PUM for all samples, with variable relative abundances among the studied xenoliths (Fig. 4; supplementary Fig. S3).

5. Discussion

5.1. The effects of primary and secondary processes on Re/Os systematics

The analysis of a large set of peridotite xenoliths from Venetia allows a critical examination of their Re-Os systematics and potentially permits discrimination between primary signatures and metasomatic alteration. On the basis of $^{187}Os/^{188}Os$ and Re-Os contents, the Venetia xenoliths can be divided into five distinct groups. Group I samples have positively correlated Re (14 – 304 ppt) and Os (0.75 – 6.5 ppb) contents and have Re/Os between 0.01 and 0.04 (Fig. 2). This group comprises four High-T harzburgites and nine Low-T lherzolites that have Re contents and $^{187}Re/^{188}Os$ that are lower than the estimated PUM and ACM values, consistent with being refractory residua (e.g., Aulbach et al., 2016). The low $^{187}Os/^{188}Os$ among group I samples (0.108-0.114, one Low-T lherzolite at 0.1186) suggests that melt depletion occurred in the Archaean. Group I samples yield realistic T_{MA} ages (i.e., within the age of the Earth) that range from 2.91 to 3.81 Ga and yield a mean T_{MA} age of 3.28 ± 0.17 Ga (95% confidence interval, MSWD = 7.8 assuming a 2σ error of 200 Myr on individual T_{MA} ages). In an $^{187}Os/^{188}Os$ versus $^{187}Re/^{188}Os$ isochron diagram (Fig. 3), the group I samples cluster tightly around the mean

T_{MA} 3.28 Ga reference line that passes through chondritic mantle (Walker et al., 2002). A regression of these samples yields an identical age to the mean T_{MA} age but has a large uncertainty due to the limited spread in $^{187}Re/^{188}Os$: 3.40 ± 1.60 Ga with an initial $^{187}Os/^{188}Os$ of 0.1047 (MSWD = 40) that is close to the chondritic model reservoir at the time $\gamma Os_{(3.4Ga)}$ = 1.0, where $\gamma Os = ((^{187}Os/^{188}Os_{sample}/ {}^{187}Os/^{188}Os_{reference})-1)*100$ at a given time. Hence, the assumption of a protolith within the chondritic range (intermediate Re/Os between PUM and ACM) appears plausible. We use the mean T_{MA} age of 3.28 ± 0.17 Ga as the best constraint on the timing of Re and Os mobility in mantle environs (i.e., the timing of craton stabilisation). The validity of this age and the interpretation of the isochronous relationship are further discussed in section 5.2.

Five Low-T lherzolites, one High-T harzburgite, one High-T lherzolite and olivine websterite ATC 727 constitute the group II samples. These samples roughly overlap in Os content (1.1 - 4.4 ppb) and $^{187}Os/^{188}Os$ (0.107 – 0.112) with the group I samples, but have distinctly higher $^{187}Re/^{188}Os$ (mostly 0.24 - 0.33) reflecting their higher Re concentrations (generally 79 - 299 ppt). Low-T lherzolite ATC 731 has the highest Re content of the sample set (1033 ppt) resulting in a $^{187}Re/^{188}Os$ of 1.67 coupled with unradiogenic $^{187}Os/^{188}Os_{EA}$ ($^{187}Os/^{188}Os$ at kimberlite eruption age; 533 Ma) similar to those of group I and other group II samples. As a result of the elevated $^{187}Re/^{188}Os$, the group II samples yield spurious T_{MA} ages that are older than the age of the Earth, whereas T_{RD} ages are indistinguishable from those of the group I samples at ~2.6 Ga (Table 1). The overlap in Os contents and $^{187}Os/^{188}Os_{EA}$ suggests that the group II samples shared a common history with the group I samples but suffered Re contamination associated with kimberlite magmatism (Fig. 3; Walker et al., 1989; Pearson et al., 1995; Carlson, 2005).

Group III comprises a Low-T lherzolite and High-T harzburgite sample that have lower Re contents than most group I and II xenoliths (46 and 65 ppt), but over an order of magnitude lower Os contents (<150 ppt). Due to the low Os content, these samples have high $^{187}Re/^{188}Os$ (~2.1) but nevertheless have sub-chondritic measured $^{187}Os/^{188}Os$ (~0.124). Group III samples yield future T_{MA} ages, but their T_{RD} ages of 3.17 and 3.31 Ga are indistinguishable from the mean T_{MA} age of the group I xenoliths. As their $^{187}Os/^{188}Os_{EA}$ overlaps with the initial of the 3.28 Ga mean T_{MA} age for group I (Fig. 3), it appears that the group III samples acquired Re during kimberlite entrainment. This is similar to the group II xenoliths, but with the major difference that Re was added to peridotites that contained essentially no Re and very little Os prior to contamination. Two important conclusions can be drawn on the basis of the unradiogenic $^{187}Os/^{188}Os_{EA}$ and the fact that these Os-poor xenoliths are especially vulnerable to overprinting. First, they have retained their Archaean depletion signature without modification for nearly 3 Gyr until entrainment in the kimberlite; and second, kimberlite contamination did not introduce significant radiogenic Os to the xenoliths. Basalt-hosted xenolith suites commonly have variable and lower Os contents than xenoliths entrained by kimberlites. This has been attributed to supergene weathering (e.g., Handler et al., 1999) or sulphide breakdown in response to interaction with S-undersaturated melts (Rudnick and Walker, 2009). The two samples (AT 1324 and AT 1338) have similar compositions and identical $^{187}Os/^{188}Os_{EA}$ to the initial of the group I isochronous regression. Hence, if Os loss occurred in these samples, then it must have been coupled to Re gain at ~533 Ma. It appears unlikely that the unradiogenic $^{187}Os/^{188}Os_{EA}$ of these two samples are the result of late stage alteration. We therefore interpret the samples as having experienced a protracted, Re-free evolution at low Os concentrations.

Whereas the group III samples are characterised by low Os contents, group IV samples are distinguished by negligible Re contents (<25 ppt) coupled with 2.7 - 6.2 ppb Os. Group IV comprises two Low-T lherzolites, one High-T harzburgite and one High-T lherzolite (Table 1). As a result of the low Re contents, T_{RD} and T_{MA} ages are identical but show considerable scatter, from 2.7 to 1.3 Ga. It appears that these group IV xenoliths have suffered major Re loss probably due to weathering and sulphide breakdown. Indeed, three out of four samples in group IV are from the Carlson et al. (1999) study that only had access to highly weathered xenoliths from the hypabyssal part of the kimberlite diatreme (Stiefenhofer et al., 1999), whereas our new samples are derived from deeper mining levels and drill cores.

Group V samples have even more disturbed Re-Os systematics. This group exclusively contains High-T lherzolite samples with low olivine Mg# (<91.6; Table 1). Rhenium concentrations (222 - 821 ppt) are among the highest of the analysed samples and Os contents are highly variable (3.05 - 11.3 ppb). $^{187}Os/^{188}Os$ displays a broad range (0.106 - 0.121), resulting in unrealistic T_{MA} ages and T_{RD} ages that are mostly <2 Ga and thus overlap with values characteristic of the convecting upper mantle (e.g., Snow & Reisberg 1995; Parkinson et al., 1998; Liu et al., 2008). One group V High-T lherzolite (V63; Carlson et al., 1999) records the oldest T_{RD} age (3.65 Ga), potentially representing a remnant of older melt depletion in the Venetian lithospheric mantle. This interpretation, however, would be based on a single sample that is part of the melt-metasomatised High-T lherzolite suite. Without other data supporting a ~3.65 Ga age at present, we cannot comment further on its possible significance. Because Re/Os systematics of the group IV and V samples are significantly disturbed and have variable T_{RD} ages (1.29 - 3.65 Ga) and unrealistic T_{MA} ages, these samples are excluded from further discussion.

Garnet clinopyroxenite sample AT 1198 does not represent a residual lithology and has a T_{MA} age (2.62 Ga) that does not correspond to the ages recorded by groups I, II and III. Furthermore, it is difficult to assess if the Re/Os of this sample was altered by kimberlite-related contamination. If any Re was added after the formation of this pyroxenite then the T_{MA} age underestimates the actual formation age. It should therefore be considered as a minimum age for this sample.

5.2. Age constraints

5.2.1. Significance of the Re/Os age

The Venetia group I samples display a strong correlation in an $^{187}Os/^{188}Os$ versus $^{187}Re/^{188}Os$ diagram and scatter around a 3.28 Ga reference line (Fig. 3). As this reference line is based on the mean T_{MA} age (3.28 ± 0.17 Ga) of the group I samples and does not reflect an actual regression of the data, it cannot be regarded as an isochron. Nevertheless, it is evident that the group I samples display an approximately isochronous relationship and it would be unrealistic to expect perfect initial isotopic equilibration over a lithospheric mantle column of >100 km (Table 1 and supplementary Fig. S1). Such a linear correlation potentially reflects radiogenic ingrowth at different parent-daughter ratios from a reservoir with initially broadly homogeneous $^{187}Os/^{188}Os$, and thus dates the time since the samples were last isotopically equilibrated. Alternatively, linear trends can result from later mixing between reservoirs with distinct isotope compositions, in which case the isochron age generally

has no significance. The isochronous relationship of the group I samples does not appear to represent a mixing line for several reasons. First, $^{187}Os/^{188}Os$ does not correlate with the reciprocal Os concentration among the group I samples (supplementary Fig. S4), which would be expected in case of mixing. Second, it is difficult to envisage a process that would lead to perfect Re-Os mixing in the lithospheric mantle. Metasomatic processes commonly introduce either Re and/or radiogenic Os to depleted mantle residua, but rarely reflect simple two-component bulk mixing relationships (e.g., Rudnick and Walker, 2009; Aulbach et al., 2016). The only mixing process that could produce the observed correlation is solid-solid mixing of a depleted, low Re/Os reservoir with primitive mantle material or enriched mantle domains such as pyroxenites. This process is difficult to accomplish from a geodynamical point of view and inconsistent with the refractory nature of the Venetia xenoliths.

Even in the unlikely instance that the isochronous relationship of the group I samples does reflect solid-solid mixing of different mantle domains, a low Re/Os reservoir with unradiogenic $^{187}Os/^{188}Os$ (0.1046 at Re/Os = 0) is still required. Such a reservoir has a model age of 3.3 Ga – equivalent to the mean T_{MA} age for the group I samples and T_{RD} age of group III. Hence, we conclude that the tight positive correlation of the group I samples in the isochron diagram testifies to the formation of the Venetia lithospheric mantle at 3.3 Ga. As such, this is the first reported whole rock mantle xenolith Re-Os near-isochronous relationship yielding an Archaean age. Interaction with melts or fluids a significant time after t_0 will generally lead to disturbance of any isochronous relationship. The group II and III samples provide an example of such disturbance as they have been displaced toward higher Re/Os probably due to the infiltration of (proto-) kimberlite melts. The preservation of a nearly isochronous Archaean Re-Os relationship among the group I samples implies that these samples have effectively remained a closed system for Re-Os for >3 Gyr, despite evidence of metasomatic overprints (e.g., Hin et al., 2009; van der Meer et al., 2013). The Re-Os systematics of the Venetia samples can thus be used to place tight constraints on the timing of lithosphere formation as will be discussed in section 5.3.

5.2.2. Correlation with crustal events

The 3.28 Ga mean T_{MA} age for the Venetia xenolith suite overlaps with the oldest tectonomagmatic event in the LMB Central Zone (supplementary Fig. S2), suggesting that the formation of the local SCLM and crust were coupled (e.g. Pearson, 1999; Griffin et al., 2004). Although detrital zircon grains found in quartzites of uncertain provenance yield ages up to 3.9 Ga (Zeh et al., 2008), the oldest magmatic zircon dates range from 3.35 to 3.27 Ga (Zeh et al., 2010; also see supplementary Fig. S2), which is considered to be the age of the stabilisation of the LMB Central Zone (e.g., Millonig et al., 2008; Zeh et al., 2010; Kramers and Mouri, 2011; Rigby et al., 2011). The Paleoarchaean rocks in the Central Zone comprise the 3.31 to 3.26 Ga Sand River Gneisses (Kröner et al., 1999; Zeh et al., 2007; Zeh et al., 2010) and the 3.34 to 3.29 Ga Messina Layered Suite (Mouri et al., 2009; Zeh et al., 2010), implying two episodes of melt extraction from the mantle. A tholeiitic amphibolite from the Venetia mine area, dated at 3.31 Ga, is likely associated with the Messina Layered Suite (Chudy et al., 2008). The tonalite-trondhjemite-granodiorite (TTG) Sand River Gneisses host magmatic zircon with slightly negative $\varepsilon Hf_{(i)}$ values, suggesting these rocks formed through reworking of older, possibly Hadean mafic protocrust in

combination with juvenile magmatism (Zeh et al., 2008; Zeh et al., 2010). In contrast, positive zircon $\varepsilon Hf_{(i)}$ values in the tholeiitic Messina Layered Suite appear to represent a major juvenile contribution to the LMB crust (Zeh et al., 2010). Further support for a major pulse of mantle melting at 3.3 Ga is provided by the interpretation of ultramafic rocks potentially associated with the Messina Layered Suite as komatiites (Mouri et al., 2013). As such, the Messina Layered Suite might be derived from magmas formed during the initial melt extraction event that produced the depleted lithospheric mantle represented by the refractory Venetia xenoliths. This conclusion is valid regardless of the choice of the model reservoir (chondritic, ACM or PUM) for the Re-Os model ages.

5.3. Melt depletion and refertilisation of the Venetia SCLM

The recognition that a subset of the Venetia xenolith samples has retained coherent Re-Os systematics without modification for over 3 Gyr provides a unique opportunity to investigate the evolution of the Venetia SCLM prior to 533 Ma. In the subsequent discussion, we use the least perturbed group I, II and III samples to address the behaviour of Re and Os during melting and the timing of Si-enrichment from an Os-isotope perspective.

5.3.1. Distribution of Re and Os in the Venetia xenoliths

In order to include the group II samples in the discussion of the petrogenesis of the Venetia xenoliths, we introduce the concept of kimberlite-corrected Re contents for these samples. The isochronous relationship of the group I samples enables us to estimate the amount of Re added to the group II samples by the kimberlite. For this correction, the group II samples are assumed to have been sited on the 3.28 Ga reference line prior to kimberlite emplacement and that all excess Re was added by the kimberlite without changing the Os concentration after 3.28 Ga. By projecting the measured $^{187}Os/^{188}Os$ along 533 Ma (kimberlite age) reference lines to the 3.28 Ga mean T_{MA} age reference line, an isochron intercept $^{187}Re/^{188}Os$ can be calculated, from which Re contents can be derived (Fig. 5). If these assumptions are valid, the group II samples are effectively corrected for Re added during kimberlite eruption based on their $^{187}Os/^{188}Os_{EA}$. For consistency, the group I samples have been recalculated in the same way, but this correction was found to be negligible.

Kimberlite-corrected values for group I and II samples, excluding Low-T lherzolite ATC 747 with anomalously high Re content, display a tight correlation between Re and Os contents ($R^2 = 0.81$). Interestingly, this trend has a non-zero initial with ~260 ppt Os at Re = 0, which is within error of the Os content of the group III samples. If only group I samples are considered, an even tighter correlation is observed ($R^2 = 0.89$; ~1.2 ppb Os at Re=0), demonstrating that this trend does not result from the substantial corrections made to the group II samples. The non-zero intercept suggests that the range in Re-Os contents is unlikely to be the result of a nugget effect caused by heterogeneous distribution of a single PGE-bearing phase. Furthermore, Os/Ir_{PUM} is invariant at 1.0 ± 0.2 (Fig. 4) and does not correlate with Os content, which strongly argues against Os-loss as a result of oxidative weathering or reaction with the host melt as commonly seen in basalt-hosted peridotites (e.g., Handler et al., 1999; Pearson et al., 2004). Any potential late-stage Os-loss has to be proportional to Re-loss to preserve the isochronous relationship of the group I samples, and is therefore considered insignificant.

In contrast, we conclude that Re and Os concentrations are controlled by the relative abundance of two distinct PGE-bearing components. The first component (A) has effectively zero Re/Os and represents a small fraction of the Os budget (contributing ~260 ppt to the bulk rock Os content from the regression in Fig. 5) while the second component (B) has higher Re/Os (~0.025). All of the Re and most of the Os appear to be hosted by component B. We stress that our components A and B represent the PGE (and Re) hosting trace phases that form only a small part of the peridotite. Therefore, absolute concentrations of Re and Os illustrated in Fig. 5 are the product of the Re and Os concentrations and the abundance of the phase, and hence have no significance. In contrast Re/Os would be identical for the whole rock and the phases hosting PGE and Re.

PGE patterns are useful in further constraining the nature of the PGE-bearing phases in the two different components. Samples with 3.9-6.4 ppb Os have flat IPGE patterns and are strongly depleted in Pt, Pd and Re compared to PUM (Fig. 4), consistent with their refractory nature. The sample with the lowest Os content (2.2 ppb), group II Low-T lherzolite ATC 725, has Os/Ir similar to PUM but lower Ru/Ir and Pt/Ir (Fig. 4 and supplementary Fig. S3). Hence, Os and Ir in this sample may be hosted in Os-Ir-rich but Ru-poor grains that stabilised in response to sulphide exhaustion after >25 % melt extraction (e.g. Luguet et al., 2007; Fonseca et al., 2012). These Os-Ir-rich phases distributed throughout the peridotite xenoliths and are likely to constitute component A. Additionally, component A could (partially) be represented by silicates; olivine in particular is a potential host for some Os and Ir (e.g. Brenan et al., 2005). The other samples have similar Os/Ir_{PUM} and higher Ru and Re contents suggesting that the PGE budget is dominated by component B, which could be a distinct or multiple sulphide phase(s) and/or Re bearing Pt-Fe alloy (Wainwright et al., 2016). Similar distribution of Re and Os between different sulphide and platinum-group minerals (PGM) have been reported in off-cratonic xenoliths (e.g. Harvey et al., 2010; Ackerman et al., 2013). Two samples have $Pd/Pt_{PUM} > 1$, as well as relatively high Re/Os, suggesting that these samples underwent mild melt metasomatism (Pearson et al., 2004). This is consistent with the presence of Cu-rich sulphides hosting Pd-Pt-rich microphases in group I sample ATC 747 (see supplementary information). Assuming that these sulphides also host Re, the fact that this sample falls on the isochron constrains Re (and thus Pd) enrichment to within 10's of Myr of melt depletion. In the case of group II sample ATC 725, Pd might have been added together with Re during (proto-) kimberlitic magmatism.

5.3.2. Mobilisation of Re and Os during melt extraction

The strong correlation of $^{187}Os/^{188}Os$ and $^{187}Re/^{188}Os$ around a 3.28 Ga reference line suggests that the variation in Re/Os of the group I samples reflects a variable degree of melt depletion. Indeed, correlations between $^{187}Os/^{188}Os$ and melt depletion indices are commonly shown by xenolith suites and can be taken as evidence for melt depletion as the dominant control on Re/Os variations (e.g., Walker et al., 1989; Meisel et al., 2001; Reisberg et al., 2004). The Venetia xenoliths display weak correlations of $^{187}Os/^{188}Os_{EA}$ with several indices of the degree of melt depletion (Fig. 6). For example, the negative correlation of $^{187}Os/^{188}Os_{EA}$ for group I and II samples excluding ATC 747 with Mg# in olivine has an R^2 of 0.40. Melt metasomatism at the time of melting can also result in covariation of $^{187}Os/^{188}Os$ with Al_2O_3 due to similar bulk compatibility to Re (e.g., Reisberg and Lorand 1995; Pearson et al., 2004; Aulbach et al., 2016). For the Venetia data, a correlation is absent in the case of Al_2O_3, which is considered to result from the introduction of aluminous orthopyroxene and hence disruption

of whole rock Al_2O_3 contents (e.g., Pearson and Wittig, 2008; Aulbach, 2012; van der Meer et al., 2013). Proxies for the degree of melt depletion that are little affected by silica enrichment such as olivine Mg# and Pt/Ir correlate with $^{187}Os/^{188}Os_{EA}$, thus seemingly lending support for melt depletion as the primary cause of the observed variation in Re/Os in the group I samples (Fig. 6).

A more detailed evaluation, however, suggests that a simple single-stage melt depletion history fails to account for multiple aspects of the Re-Os systematics of the Venetia xenolith suite. Importantly, concentrations of incompatible Re and compatible Os correlate positively (Fig 2a and Fig. 5b) and Re-contents are too high to reflect residua of up to 50 % melting as implied by olivine Mg# of up to 93.6. The commonly accepted view is that Re partitions almost completely into the melt phase once sulphide is exhausted at ~25 % melting and that the unradiogenic $^{187}Os/^{188}Os$ of many cratonic xenoliths implies that any observed Re has been added recently (e.g., Pearson et al., 1995, 2004). In the case of Venetia group I samples, the preservation of the approximately isochronous relationship indicates that higher Re/Os has persisted since the Archaean and that Re was either not quantitatively lost during melting, or has been re-introduced to the refractory residue during or shortly following melt depletion. Second, the mean Os content of the Venetia group I and II xenoliths (3.8 ppb) is comparable to the average value of cratonic kimberlite-borne xenoliths (3.4 ppb) and modelled residua of ~40 % melt depletion (Aulbach et al., 2016). Individual Os contents, however, vary from 0.1 to 6.5 ppb and do not show a correlation with degree of depletion, although the variation in Os concentration increases with higher olivine Mg# (Fig. 6; Gao et al., 2002). Auto-refertilisation, a process by which Re is precipitated from the melt back into the mantle residue after a short distance of melt migration during dynamic melting (Rudnick & Walker 2009) may explain the retention of some Re at higher degrees of melt depletion. Rhenium-retention also appears possible at low pressure and oxygen fugacity (ΔFMQ-2) in the models of Aulbach et al. (2016), wherein a part of the melt is retained in the residue. A problem is that these models offer no explanation for positively correlating Re and Os concentrations and can therefore not be the only cause for the observed Re budget.

If our conclusion that the PGE budget of the Venetia xenoliths is controlled by the relative abundance of PGE-bearing components is correct, the correlation between Re and Os content reflects the relative proportion in which the two phases are present in a sample, and as such a “mixing line” between the two components (Fig. 5b). On this basis, the observed Re-Os systematics require at least two distinct mechanisms that governed the PGE budget during SCLM formation: i) initial melt depletion (melt depletion curve in Fig. 5c), resulting in covariation of Re/Os with degree of depletion; and ii) local redistribution of the PGE budget between phases A and B. After >25 % melt depletion, IPGE-rich sulphides and PGM are the expected host for PGE and Re (e.g., Lorand and Luguet, 2016). Interaction with percolating melts can transform these residual phases back to base metal sulphides and lead to mobilisation of Os and Re, leaving behind a relatively Os-poor sulphide or PGM assemblage (e.g., Alard et al., 2002; Lorand et al., 2013; Wainwright et al., 2015; Aulbach et al., 2016; Kochergina et al., 2016) that is interpreted to host Os in component A in the Venetia samples. If these locally derived percolating melts/fluids are (close to being) S-saturated, Os-rich sulphides with relatively high Re/Os could be mobilised as immiscible melt droplets without being dissolved in the melt. Upon a change in physical conditions, the sulphide melt droplets would stall elsewhere in the depleted peridotites (e.g., Pearson et al.,

2004; Kochergina et al., 2016). As a consequence, Re and Os are effectively heterogeneously redistributed in the form of component B. The samples that contain the largest proportion of component B (e.g., ATC 747) are characterised by very high IPGE contents, Pd enrichment ($Pd/Pt_{PUM} > 1$) and a higher abundance of sulphides (supplementary data). ATC 747 also has the highest $^{187}Os/^{188}Os$ and Re/Os ratios of all of the group 1 samples.

An important point is that component B exerts the dominant control on Re/Os and that mobilisation of Os will not dramatically alter Re/Os except where a substantial proportion of the Os is hosted by component A; i.e. at <1 ppb Os (Fig. 5c). The general correlation between Re/Os (and as a result $^{187}Os/^{188}Os_{EA}$) and degree of melt depletion therefore primarily reflects the difference between samples with Mg# up to 92.5 with those with higher Mg# and slightly lower Re/Os coupled with variable Re and Os concentrations due to mobilisation of component B over small distances. The timing of Os mobilisation is critically constrained to occur during or shortly after melt depletion in order to preserve the isochronous relationship. Moreover, the two group III samples with very low Os contents (~150 ppt) yield T_{RD} ages of ~3.25 Ga (Table 1) that constrain the time of Os- and Re-loss to be within error of the mean T_{MA} age. Rhenium and Os could therefore have been retained and remobilised by infiltrating melt/fluid broadly synchronous with melt extraction, a process involving local re-precipitation of sulphides after a small distance of melt migration. The orthopyroxene-rich nature of the samples, however, indicates that pervasive Si-metasomatism must be accounted for. Therefore, Re and Os may have been remobilised during a second, unrelated event shortly after initial melt extraction. This introduces the problem that we find no evidence for the introduction of radiogenic Os from a recycled source at ~3.28 Ga, a point that is discussed below.

5.3.3. Os isotopes and Si-enrichment

From petrographic and geochemical evidence, it appears that the Venetia mantle xenoliths do not represent residua of a single melt extraction episode but have witnessed extensive Si-enrichment (Hin et al., 2009; van der Meer et al., 2013) and melt metasomatism in the case of High-T lherzolites. Silicon-enrichment translates to modal orthopyroxene contents in excess of those expected for refractory residua (e.g., Walter, 1998; van der Meer et al., 2013). Venetia shares this Si-rich nature with the majority of Kaapvaal SCLM samples (e.g., Boyd, 1989), for which a wide range of models have been proposed. Most support is found for a metasomatic origin with Si addition either by intraplate melts (e.g., Koornneef et al., 2009), through interaction with Si-rich fluids or melts in a subduction zone (e.g., Kesson and Ringwood, 1989; Kelemen et al., 1998; Bell et al., 2005; Simon et al., 2007) or eclogite melting in a plume (e.g., Aulbach et al., 2011). Although the debate on the origin of high modal orthopyroxene is ongoing, Si-enrichment in cratonic xenoliths is typically associated with the introduction of radiogenic Os from a recycled component (Simon et al., 2007; Aulbach et al., 2009; 2011; 2016; Smit et al., 2014). For instance, Aulbach et al. (2011) relate orthopyroxene addition and suprachondritic initial $^{187}Os/^{188}Os$ of peridotitic sulphide inclusions in central Slave Craton diamonds to interaction with eclogite melts with radiogenic $^{187}Os/^{188}Os$. In addition, Simon et al. (2007) find a correlation between modal orthopyroxene content and $^{187}Os/^{188}Os_{EA}$ for Low-T peridotites from Kimberley (Kaapvaal Craton). These authors interpret elevated $^{187}Os/^{188}Os$ unsupported by higher Re/Os as evidence for the addition of radiogenic Os from a subducting slab, which is consistent with the occurrence of 2.9 Ga eclogitic diamond inclusions with radiogenic

initial $^{187}Os/^{188}Os$ from the same mine (Richardson et al., 2001). Pyroxenite formation in peridotite massifs has been related to the introduction of Re and radiogenic Os (e.g. van Acken et al., 2010). The two pyroxenites examined here appear to have formed in separate events. Olivine websterite ATC 727 (with 57 % modal orthopyroxene, van der Meer et al., 2013) is part of group II and appears to have had a shared development with the peridotite lithologies. Garnet clinopyroxenite AT 1198 on the other hand has high Re/Os and very radiogenic Os. The relatively young minimal T_{MA} of this sample (2.62 Ga), however, indicates that this lithology was probably related to a later magmatic event in which case its formation had no noticeable effect on the Re/Os systematics of group I, II and III samples.

The relatively pristine Re-Os systematics of the Venetia group I, II and III samples offer an ideal opportunity to investigate the nature and timing of orthopyroxene addition to the SCLM. In contrast to Simon et al. (2007), we find neither systematic variation of the range in modal orthopyroxene contents (~10 to 40 %; Fig. 7) with $^{187}Os/^{188}Os_{EA}$ nor obvious correlations with Re/Os and Os, arguing against coupled Re and/or radiogenic Os proportional to orthopyroxene addition to a refractory mantle residue. Moreover, the isochronous relationship of the Venetia samples with unradiogenic initial $^{187}Os/^{188}Os$ (~0.1046, model age ~3.3 Ga) is not compatible with the introduction of radiogenic Os. As it seems unlikely that the pervasive Si-enrichment of the SCLM could have occurred without affecting the Re/Os system in any way, there is an apparent paradox of aluminous orthopyroxene addition, derived from a recycled component, and lack of introduction of radiogenic Os. This paradox can be alleviated if the recycled component is young (at the time of introduction) and has not had time to acquire highly radiogenic $^{187}Os/^{188}Os$. This scenario requires that a limited amount of time elapsed between initial melt depletion and Si-enrichment (<100 Myr). Geological evidence supports rapid formation and stabilisation of the LMB Central Zone lithosphere associated with multiple mantle melting events. We propose a scenario in which the ~3.35 Ga tholeiitic Messina Layered suite is complementary to the depleted Venetia SCLM. We further suggest that TTG magmatism at 3.28 Ga was associated with Si-enrichment of the SCLM. Eclogite melting is proposed as the main mode of formation of TTG suites (e.g., Foley et al., 2002; Rollinson, 2010) and can thus be directly related to the stabilisation of orthopyroxene in the Venetia refractory peridotites. Moreover, as demonstrated by Zeh et al. (2010), negative zircon initial εHf of the 3.28 Ga Sand River TTG's requires recycling of crustal material. Taken together, we find that recycling of oceanic crust equivalent to the Messina Layered suite within 70 Myr satisfies both the crustal Hf isotope evidence in the form of the Sand River TTG gneisses and the lack of perturbation of $^{187}Os/^{188}Os$ in the Venetia xenoliths. The addition of up to 30 % of melts derived from tholeiitic crust (40 ppt Os, $^{187}Os/^{188}Os_{(i)}$ = 0.1041, $^{187}Re/^{188}Os$ = 23 and $^{187}Os/^{188}Os_{(i + 70Ma)}$ = 0.1309) 70 Myr after its extraction from the convecting mantle at 3.35 Ga to the Venetia refractory mantle will raise $^{187}Os/^{188}Os_{(i)}$ from 0.1046 to 0.1048. This variation is irresolvable within the uncertainty of the isochron initial $^{187}Os/^{188}Os$. Hence, our proposed "rapid recycling" model can account for the lack of radiogenic Os addition accompanying Si-enrichment of the Venetia xenoliths. In contrast, amalgamation, and likely Si-enrichment, of the Kaapvaal Craton (Kimberley) at 2.9 Ga postdates the main mantle melting episode by 300 - 400 Myr (Richardson et al., 2001; Shirey et al., 2002; Simon et al., 2007). The time gap is even larger in the central Slave Craton (Aulbach et al., 2009; Aulbach et al., 2011), leaving sufficient time for highly radiogenic Os compositions to develop in the mafic crust that was recycled, ultimately

sourcing melt/fluids that metasomatised the SCLM. These significant time gaps between initial melting and orthopyroxene metasomatism allow the introduction of radiogenic Os, which offers a possible explanation as to why Re-Os isochronous relationships are not preserved in Kimberley and Slave Craton peridotite suites.

5.3.4. The evolution of the Venetia SCLM

The geodynamical setting of melt extraction and mode of recycling of the Messina Layered suite cannot be tightly constrained by the Re-Os data alone and hence a detailed examination falls outside the scope of this study. Nevertheless, the preceding discussion allows some inferences to be made on the evolution of the Limpopo SCLM. In order to stimulate further research, we will present a geodynamical model based on the Re-Os systematics whilst acknowledging that more data are required to substantiate the model.

A primary observation is that samples with the lowest olivine Mg# (<92.3) and lowest modal orthopyroxene contents best approximate a ~30% melt depleted residue in terms of their Re and Os contents and Mg# (Figures 5c and 7b). The lack of correlation of orthopyroxene content with Re, Os, and Os-isotope compositions suggests that Re-Os mobilisation was not directly related to silicate mineralogy. It is striking, however, that the samples with olivine Mg# less than ~92.5 show a significantly smaller variation in Os contents than samples with olivine Mg# >92.5. On this basis, we propose a two-stage model that is illustrated in Fig. 8. The model comprises an initial episode of ~30 % melt extraction at 3.35 Ga to produce a harzburgitic residue with olivine Mg# ~92.3 and a ~30 km thick complementary mafic crust (Herzberg and Rudnick, 2012). If melting occurred at relatively low pressure and reducing conditions in an oceanic ridge setting, Re might not be quantitatively lost to the melt (Fig. 5c and 7b; Aulbach et al., 2016). Additionally, auto-refertilisation during dynamic melting processes might leave higher Re/Os than simple melt extraction (Rudnick and Walker 2009). Melt extraction from newly formed crust 70 Myr later, after transport to depth during accretion (probably in a slab-stacking or subduction-like setting) would result in an additional ~10 to 15 % hydrous melting of the lithospheric mantle, thereby raising olivine Mg# to 93.5 and stabilising aluminous orthopyroxene. Both of these melting events could create a small range of Re/Os, necessary for the development of an isochron. If the eclogite-derived melts of the latter event were (close to being) S saturated, residual sulphides (i.e. component B) might be locally remobilised as immiscible melt droplets but need not necessarily be dissolved in the melt and hence lost from the mantle (e.g., Pearson et al., 2004; Reisberg et al., 2004). This scenario could explain the correlation between (kimberlite-corrected) Re and Os concentrations in the group I and II Venetia xenoliths. Part of the lithosphere has apparently not, or only to a minor extent, witnessed the second melt extraction and Si-enrichment event, as indicated by the persistence of the samples with lower olivine Mg# and less disrupted Re-Os systematics. Based on the lack of radiogenic Os addition, we argue that the mode of crustal recycling leading to TTG magmatism and Si-enrichment is inconsistent with eclogite entrainment and melting in an upwelling plume (e.g. Aulbach et al., 2011). The 70 Myr time gap is insufficient to account for recycling of mafic crust to the lower mantle and back. Instead, rapid recycling was achieved either through an Archean equivalent of subduction (e.g., Pearson and Wittig, 2008), subcretion of oceanic crust beneath Craton margins (e.g. Bédard, 2017) or foundering of eclogite keels of thick oceanic crust (e.g., Bédard, 2006). Considering that Os mobility is most easily achieved in a hydrous, oxidising environment (e.g., Brandon et al., 1996; Alard et al.,

2002; Aulbach et al., 2016), we find most support for recycling though an Archean equivalent of subduction or slab stacking but clearly additional data are required to support this interpretation. Stacking or imbrication of lithospheric mantle does, however, explain the lack of correlation between equilibration pressure of the xenoliths and degree of melt depletion, $^{187}Os/^{188}Os_{EA}$ and Re and Os contents (Supplementary Fig. S1). Eclogite xenoliths are extremely rare in the Venetia xenolith suite and analyses are lacking, thus leaving no independent means to constrain the timing and nature of lithospheric recycling in the LMB.

Following rapid lithosphere stabilisation between 3.35 and 3.28 Ga, the majority of the Venetia samples have remained a closed system for Re and Os until entrainment in the host kimberlite at 533 Ma, despite evidence for multiple Neoarchaean and Proterozoic tectonomagmatic events (e.g., Zeh et al., 2010). The collision between the Zimbabwe and Kaapvaal Cratons at ~2.65 Ga (e.g., Zeh et al., 2007; Millonig et al., 2008; Kramers and Mouri, 2011) apparently left no trace in the Re-Os systematics of the peridotite xenoliths. In contrast, if the 2.62 Ga T_{MA} of the highly radiogenic garnet-clinopyroxenite (Figure 2) represents its formation age then it is indistinguishable from the collision age indicating melt migration through the lithosphere at this time. The strong metamorphic overprint at ~2.0 Ga in the LMB crust, roughly coeval with but unrelated to Bushveld magmatism (e.g., Zeh et al., 2007; Chudy et al., 2008), is also unrecorded by the Venetia peridotite xenoliths. This age, however, is recorded in eclogitic sulphide diamond inclusions from Venetia (Richardson and Shirey, 2008), which scatter around a 2.05 Ga Re-Os isochron with an initial $^{187}Os/^{188}Os$ that is more radiogenic (~0.25) than Bushveld magmas or any of the Venetia xenoliths (Richardson and Shirey, 2008). Hence, the eclogitic sulphide inclusions provide evidence for at least localised introduction of radiogenic Os to the deep, diamondiferous keel of the Venetia SCLM. In order to reconcile the lack of a pervasive Os overprint with the evidence for pronounced metasomatic events at ~2 Ga and possibly ~2.6 Ga, we propose that these later melts were spatially limited to metasomes that would have formed along their pathways and did not invade the entire SCLM, leaving in particular the low-T suite unaffected. Phanerozoic metasomatism (after the emplacement of the Venetia kimberlite) related to Karoo flood basalts and regional kimberlites appears to have been more pervasive throughout the SCLM, explaining why samples from younger kimberlites do not display isochronous behaviour. Additionally, sulphide-bearing, relatively fertile peridotites at the base of the lithosphere could effectively scavenge Re and PGEs from melts that infiltrate the SCLM, leaving melts that reach higher levels PGE-bare (e.g., Reisberg et al., 2004). In this scenario, percolating melts have the potential to affect lithophile elements in the upper SCLM but have negligible influence on the Re-Os systematics. A sulphide-bearing boundary layer at the base of the SCLM could thus form an effective shield against melt metasomatism for the Re-Os system. PGE scavenging is consistent with the generally high Os (up to 11.3 ppb) contents and variably radiogenic $^{187}Os/^{188}Os$ (0.106 – 0.121) of the High-T lherzolites and some High-T harzburgite samples (groups IV and V), which are interpreted to have equilibrated with melts derived from the convecting mantle (e.g., Lorand et al., 2013; Aulbach et al., 2016). The preservation of the isochronous relationship in multiple High-T samples (Table 1 and supplementary Fig. S1) indicates that the deep SCLM was not uniformly overprinted, but that interaction with silicate melts after ~3.3. Ga SCLM stabilisation appears to have been confined to veins or discrete zones. Furthermore, we find no evidence in the xenolith suite for the

presence of eclogitic pods with radiogenic Os compositions proposed by Richardson and Shirey (2008) to exist in the SCLM, with perhaps the exception of pyroxenite formation at ≥2.62 Ga.

5.4. Significance of T_{RD} and T_{MA} model ages

Due to the ubiquity of metasomatic overprint on the Re-Os systematics in cratonic xenoliths, isochronous relationships are generally not preserved and T_{RD} and T_{MA} model ages are used to constrain the timing of melt depletion (e.g., Walker et al., 1989; Pearson et al., 1995; Rudnick and Walker, 2009; Pearson and Wittig, 2014). Although T_{RD} ages must be interpreted as *minimum* ages, it is generally assumed that Re has been quantitatively extracted during melting in highly refractory samples. In consequence, T_{RD} ages are commonly correlated with crustal events (e.g., Pearson and Wittig, 2008, 2014). In this study, we have demonstrated that the Venetia xenoliths are characterised by long-term elevated Re/Os, implying that a significant amount of Re was present since lithosphere stabilisation at ~3.3 Ga despite olivine Mg# indicating >30% melt extraction. Rhenium was retained during the initial melting event, and/or added during TTG magmatism <70 My later. Rhenium-depletion ages therefore clearly underestimate the true depletion age of the xenoliths. This is illustrated in Fig. 9, where $^{187}Os/^{188}Os$ evolution with time and histograms of both T_{MA} and T_{RD} ages are presented (see also Table 1). Group II samples, characterised by mild Re addition during kimberlite entrainment, yield T_{MA} ages in excess of the age of the Earth but their $^{187}Os/^{188}Os_{EA}$ and T_{RD} ages are identical to those of group I samples, with an average age of ~2.6 ± 0.2 Ga, much younger than the ~3.3 Ga mean T_{MA} age that is supported by the isochronous relationship. Venetia T_{RD} ages therefore convey no meaningful absolute age information. If the group I samples had not shown the tight correlation in an isochron diagram, one could easily have interpreted the 2.6 Ga mean T_{RD} age of the group I and II samples as lithosphere stabilisation during the 2.65 Ga Kaapvaal-Limpopo amalgamation. The correspondence of the mean T_{RD} age with this tectonomagmatic event is, however, purely fortuitous and has no geological significance. The only Re-Os data suggestive of a ~2.6 Ga event is the T_{MA} age of the very radiogenic garnet-clinopyroxenite AT 1198. The two group III samples that have lost all Re and most of their Os during SCLM stabilisation are the only peridotites in this study that yield meaningful T_{RD} ages of ~3.2 Ga (Fig. 9). This study underscores the importance of acquiring a sufficiently large dataset to allow scrutiny of the results in order to extract reliable age information (e.g., Rudnick and Walker, 2009; Pearson and Wittig, 2014; Liu et al., 2016).

Finally, it is important to stress that there is increasing evidence for significant primary Re contents in highly depleted peridotites. Recent melt depletion modelling by Aulbach et al. (2016) allows for significant residual Re following low pressure melting under reducing conditions, even up to 40 %. Non-zero primary Re is also increasingly recognised in highly depleted off-craton xenolith samples where T_{RD} ages appear to significantly underestimate the actual age of depletion (e.g., Janney et al., 2010; Kochergina et al., 2016) and is inferred by correlation of T_{RD} ages with the degree of PPGE depletion (Pearson et al., 2002; Aulbach et al., 2016). Although primary Re contents of the Venetia xenoliths are slightly higher than those of average depleted Kaapvaal xenoliths, the Venetia samples are very similar in terms of chemistry, petrology and Re-Os isotope composition and both sample suites record a clear dichotomy between T_{RD} and T_{MA} ages (Pearson and Wittig

2014). Whole rock T_{RD} ages from Kaapvaal show a well-defined mode at ~2.7 Ga with few T_{RD} ages >3.0 Ga, whereas sulphide T_{MA} ages have maxima at ~3.1 and ~2.7 Ga (Griffin et al., 2004; Pearson and Wittig, 2008, 2014). This difference was variably interpreted to either reflect metasomatic overprint of the whole rocks that thus yield mixed ages (Griffin et al., 2004) or as lithosphere stabilisation in the Neoarchaean at 2.9 Ga following craton amalgamation (Pearson and Wittig, 2014). Non-zero primary Re contents in residua provide an alternative explanation for the systematically younger T_{RD} ages. Support for this interpretation is provided by >3.0 Ga T_{MA} ages of the most depleted, lowest Re/Os sulphides (Griffin et al., 2004) and the least radiogenic Kimberley xenoliths (Simon et al., 2007), as well as 3.3 Ga Sm-Nd model ages for silicate diamond inclusions (Richardson et al., 1984). Quantitative Re extraction during the formation of Archaean refractory mantle might thus not be as universal as commonly accepted, implying that lithospheric keels are much older than inferred on the basis of peaks in the distribution of T_{RD} ages.

6. Conclusions

A detailed Re-Os isotope study of mantle xenoliths from the 533 Ma Venetia kimberlite cluster in the Limpopo Mobile Belt, South Africa establishes that:

1. The Venetia xenoliths can be divided into five groups on the basis of Re and Os contents and $^{187}Os/^{188}Os$, ranging from pristine group I samples to highly disturbed group V samples. The group I samples yield a mean T_{MA} age of 3.28 ± 0.17 Ga and display an approximately isochronous relationship of the same age that passes through mantle reference values; group II samples are interpreted to have been on the isochron until minor Re addition during kimberlite magmatism.
2. The near isochronous relationship of the group I samples indicates that the Venetia xenoliths have higher Re/Os than expected for residua of 40 % melt depletion, which cannot result from recent Re addition. Such high Re contents may partially reflect low-pressure melting under reducing conditions and/or auto-refertilisation during dynamic melting. In addition, the highly variable Os contents suggest remobilisation of Re and Os during or shortly after initial melt depletion.
3. Silicon-enrichment of the Venetia xenoliths requires a contribution from recycled crust. The absence of introduced radiogenic Os and preservation of the isochronous relationship constrains Si-enrichment and Re-Os remobilisation to <100 Myr of initial melt depletion.
4. We propose a rapid recycling model with initial melt depletion at 3.35 Ga to form a tholeiitic mafic crust (Messina Layered suite) that is recycled at ~3.28 Ga, resulting in the intrusion of a TTG suite (Sand River gneisses) and Si-enrichment of the lithospheric mantle. Hence, formation and stabilisation of the Limpopo lithosphere was achieved within 70 Myr in the Mesoarchaean, in contrast to the more protracted history of the Kaapvaal SCLM.
5. The high primary Re contents of the Venetia xenoliths imply that T_{RD} model ages significantly underestimate the true age of melt depletion; the overlap of the mean T_{RD} age with the Kaapvaal-Limpopo collision is purely fortuitous and the T_{RD} ages have no geological significance. A growing body

of evidence for non-zero primary Re contents in highly depleted cratonic mantle warrants a critical re-evaluation of the use of T_{RD} ages as a tool to date lithosphere formation.

Acknowledgements

We greatly acknowledge the help of Catherine Zimmermann in obtaining the Re-Os data. DeBeers and the Venetia mine staff are thanked for providing access to the mine and assistance in the field. Rick Carlson and Ian Parkinson are thanked for fruitful discussions and Armin Zeh kindly shared his expert knowledge on the tectonomagmatic history of the Limpopo Mobile Belt. David van Acken, Sonja Aulbach and an anonymous reviewer provided constructive reviews that helped focus the manuscript. Alan Brandon is thanked for editorial handling. Financial support for the Re-Os analyses was provided through Europlanet-RI and the Dr. Schürmann Foundation covered fieldwork expenses. Europlanet 2020 RI has received funding from the European Union's Horizon 2020 research and innovation programme under grant agreement No 654208. The research leading to these results has received funding from the European Research Council under the European Union's Seventh Framework Programme (FP7/2007-2013)/ERC grant agreement no. 319209.

References

Ackerman, L., Pitcher, L., Strnad, L., Puchtel, I.S., Jelínek, E., Walker, R.J. and Rohovec, J. (2013) Highly siderophile element geochemistry of peridotites and pyroxenites from Horní Bory, Bohemian Massif: Implications for HSE behaviour in subduction-related upper mantle. *Geochim. Cosmochim. Acta* **100**, 158-175.

Alard, O., Griffin, W.L., Pearson, N.J., Lorand, J.-P. and O'Reilly, S.Y. (2002) New insights into the Re–Os systematics of sub-continental lithospheric mantle from in situ analysis of sulphides. *Earth Planet. Sci. Lett.* **203**, 651-663.

Allsopp, H., Smith, C., Seggie, A., Skinner, E. and Colgan, E. (1995) The emplacement age and geochemical character of the Venetia kimberlite bodies, Limpopo Belt, northern Transvaal. *S. Afr. J. Geol.* **98**, 239-244.

Aulbach, S. (2012) Craton nucleation and formation of thick lithospheric roots. *Lithos* **149**, 16-30.

Aulbach, S., Creaser, R.A., Pearson, N.J., Simonetti, S.S., Heaman, L.M., Griffin, W.L. and Stachel, T. (2009) Sulfide and whole rock Re–Os systematics of eclogite and pyroxenite xenoliths from the Slave Craton, Canada. *Earth Planet. Sci. Lett.* **283**, 48-58.

Aulbach, S., Mungall, J.E. and Pearson, D.G. (2016) Distribution and processing of highly siderophile elements in cratonic mantle lithosphere. *Rev. Mineral. Geochem.* **81**, 239-304.

Aulbach, S., Stachel, T., Heaman, L.M., Creaser, R.A. and Shirey, S.B. (2011) Formation of cratonic subcontinental lithospheric mantle and complementary komatiite from hybrid plume sources. *Contrib. Mineral. Petrol.* **161**, 947-960.

Aulbach, S., Stachel, T., Viljoen, S.K., Brey, G.P. and Harris, J.W. (2002) Eclogitic and websteritic diamond sources beneath the Limpopo Belt–is slab-melting the link? *Contrib. Mineral. Petrol.* **143**, 56-70.

Barton, J. and Gerya, T. (2003) Mylonitization and decomposition of garnet: evidence for rapid deformation and entrainment of mantle garnet-harzburgite by kimberlite magma, K1 Pipe, Venetia Mine, South Africa. *S. Afr. J. Geol.* **106**, 231-242.

Becker, H., Horan, M., Walker, R., Gao, S., Lorand, J.-P. and Rudnick, R. (2006) Highly siderophile element composition of the Earth's primitive upper mantle: constraints from new data on peridotite massifs and xenoliths. *Geochim. Cosmochim. Acta* **70**, 4528-4550.

Bédard, J.H. (2006) A catalytic delamination-driven model for coupled genesis of Archaean crust and sub-continental lithospheric mantle. *Geochim. Cosmochim. Acta* **70**, 1188-1214.

Bédard, J.H. (2017) Stagnant lids and mantle overturns: Implications for Archaean tectonics, magmagenesis, crustal growth, mantle evolution, and the start of plate tectonics. *Geoscience Frontiers.*

Bell, D., Gregoire, M., Grove, T., Chatterjee, N., Carlson, R. and Buseck, P. (2005) Silica and volatile-element metasomatism of Archean mantle: a xenolith-scale example from the Kaapvaal Craton. *Contrib. Mineral. Petrol.* **150**, 251-267.

Bernstein, S., Kelemen, P.B. and Hanghøj, K. (2007) Consistent olivine Mg# in cratonic mantle reflects Archean mantle melting to the exhaustion of orthopyroxene. *Geology* **35**, 459-462.

Birck, J.L., Barman, M.R. and Capmas, F. (1997) Re-Os Isotopic Measurements at the Femtomole Level in Natural Samples. *Geostand. Newslett.* **21**, 19-27.

Boyd, F. (1989) Compositional distinction between oceanic and cratonic lithosphere. *Earth Planet. Sci. Lett.* **96**, 15-26.

Brandon, A.D., Creaser, R.A., Shirey, S.B. and Carlson, R.W. (1996) Osmium recycling in subduction zones. *Science* **272**, 861.

Brenan, J.M., McDonough, W.F. and Ash, R. (2005) An experimental study of the solubility and partitioning of iridium, osmium and gold between olivine and silicate melt. *Earth and Planetary Science Letters* **237**, 855-872.

Carlson, R., Pearson, D., Boyd, F., Shirey, S., Irvine, G., Menzies, A. and Gurney, J. (1999) Re–Os systematics of lithospheric peridotites: implications for lithosphere formation and preservation, The JB Dawson Volume—

Proceedings of the Seventh International Kimberlite Conference, Cape Town. Red Roof Design, Cape Town, pp. 99-108.

Carlson, R.W. (2005) Application of the Pt–Re–Os isotopic systems to mantle geochemistry and geochronology. *Lithos* **82**, 249-272.

Chudy, T., Zeh, A., Gerdes, A., Klemd, R. and Barton, J. (2008) Palaeoarchaean (3.3 Ga) mafic magmatism and Palaeoproterozoic (2.02 Ga) amphibolite-facies metamorphism in the Central Zone of the Limpopo Belt: New geochronological, petrological and geochemical constraints from metabasic and metapelitic rocks from the Venetia area. *S. Afr. J. Geol.* **111**, 387-408.

Creaser, R., Papanastassiou, D. and Wasserburg, G. (1991) Negative thermal ion mass spectrometry of osmium, rhenium and iridium. *Geochim. Cosmochim. Acta* **55**, 397-401.

Dale, C.W., Macpherson, C.G., Pearson, D.G., Hammond, S.J. and Arculus, R. J. (2012) Inter-element fractionation of highly siderophile elements in the Tonga Arc due to flux melting of a depleted source. *Geochim. Cosmochim. Acta* **89**, 202-225.

de Wit, M.J., de Ronde, C.E., Tredoux, M., Roering, C., Hart, R.J., Armstrong, R.A., de Ronde, C.E.J., Green, R.W.E., Tredoux, M., Peberdy, E. and Hart, R.A. (1992) Formation of an Archaean continent. *Nature* **357**(6379), 553-562.

Foley, S., Tiepolo, M. and Vannucci, R. (2002) Growth of early continental crust controlled by melting of amphibolite in subduction zones. *Nature* **417**, 837-840.

Fonseca, R.O., Laurenz, V., Mallmann, G., Luguet, A., Hoehne, N. and Jochum, K.P. (2012) New constraints on the genesis and long-term stability of Os-rich alloys in the Earth's mantle. *Geochim. Cosmochim. Acta* **87**, 227-242.

Gao, S., Rudnick, R.L., Carlson, R.W., McDonough, W.F. and Liu, Y.-S. (2002) Re–Os evidence for replacement of ancient mantle lithosphere beneath the North China craton. *Earth Planet. Sci. Lett.* **198**, 307-322.

Giuliani, A., Phillips, D., Maas, R., Woodhead, J.D., Kendrick, M.A., Greig, A., Armstrong, R.A., Chew, D., Kamenetsky, V.S. and Fiorentini, M.L. (2014) LIMA U–Pb ages link lithospheric mantle metasomatism to Karoo magmatism beneath the Kimberley region, South Africa. *Earth Planet. Sci. Lett.* **401**, 132-147.

Grégoire, M., Bell, D. and Le Roex, A. (2003) Garnet lherzolites from the Kaapvaal Craton (South Africa): trace element evidence for a metasomatic history. *J. Petrol.* **44**, 629-657.

Griffin, W., Graham, S., O'Reilly, S.Y. and Pearson, N. (2004) Lithosphere evolution beneath the Kaapvaal Craton: Re–Os systematics of sulfides in mantle-derived peridotites. *Chem. Geol.* **208**, 89-118.

Handler, M.R., Bennett, V.C. and Dreibus, G. (1999) Evidence from correlated Ir/Os and Cu/S for late-stage Os mobility in peridotite xenoliths: Implications for Re-Os systematics. *Geology* **27**, 75-78.

Harvey, J., Gannoun, A., Burton, K., Schiano, P., Rogers, N. and Alard, O. (2010) Unravelling the effects of melt depletion and secondary infiltration on mantle Re–Os isotopes beneath the French Massif Central. *Geochim. Cosmochim. Acta* **74**, 293-320.

Herzberg, C. and Rudnick, R. (2012) Formation of cratonic lithosphere: An integrated thermal and petrological model. *Lithos* **149**, 4-15.

Hin, R., Morel, M., Nebel, O., Mason, P., van Westrenen, W. and Davies, G. (2009) Formation and temporal evolution of the Kalahari sub-cratonic lithospheric mantle: Constraints from Venetia xenoliths, South Africa. *Lithos* **112**, 1069-1082.

Ishikawa, A., Senda, R., Suzuki, K., Dale, C.W. and Meisel, T. (2014) Re-evaluating digestion methods for highly siderophile element and 187 Os isotope analysis: Evidence from geological reference materials. *Chemical Geology* **384**, 27-46.

James, D., Fouch, M., VanDecar, J. and Van Der Lee, S. (2001) Tectospheric structure beneath southern Africa. *Geophys. Res. Lett.* **28**, 2485-2488.

Janney, P., Shirey, S., Carlson, R., Pearson, D., Bell, D., Le Roex, A., Ishikawa, A., Nixon, P. and Boyd, F. (2010) Age, composition and thermal characteristics of South African off-craton mantle lithosphere: Evidence for a multi-stage history. *J. Petrol.* **51**, 1849-1890.

Kelemen, P.B., Hart, S.R. and Bernstein, S. (1998) Silica enrichment in the continental upper mantle via melt/rock reaction. *Earth Planet. Sci. Lett.* **164**, 387-406.

Kesson, S. and Ringwood, A. (1989) Slab-mantle interactions: 2. The formation of diamonds. *Chem. Geol.* **78**, 97-118.

Khoza, D., Jones, A., Muller, M., Evans, R., Webb, S. and Miensopust, M. (2013) Tectonic model of the Limpopo belt: Constraints from magnetotelluric data. *Precambrian Res.* **226**, 143-156.

Kobussen, A.F., Griffin, W.L. and O'Reilly, S.Y. (2009) Cretaceous thermo-chemical modification of the Kaapvaal cratonic lithosphere, South Africa. *Lithos* **112**, 886-895.

Kochergina, Y.V., Ackerman, L., Erban, V., Matusiak-Małek, M., Puziewicz, J., Halodová, P., Špaček, P., Trubač, J. and Magna, T. (2016) Rhenium–osmium isotopes in pervasively metasomatized mantle xenoliths from the Bohemian Massif and implications for the reliability of Os model ages. *Chem. Geol.* **430**, 90-107.

Koornneef, J.M., Davies, G.R., Döpp, S.P., Vukmanovic, Z., Nikogosian, I.K. and Mason, P.R. (2009) Nature and timing of multiple metasomatic events in the sub-cratonic lithosphere beneath Labait, Tanzania. *Lithos* **112**, 896-912.

Kramers, J.D. and Mouri, H. (2011) The geochronology of the Limpopo Complex: a controversy solved. *Geological Society of America Memoirs* **207**, 85-106.

Kröner, A., Jaeckel, P., Brandl, G., Nemchin, A. and Pidgeon, R. (1999) Single zircon ages for granitoid gneisses in the Central Zone of the Limpopo Belt, Southern Africa and geodynamic significance. *Precambrian Res.* **93**, 299-337.

Liu, C.Z., Snow, J.E., Hellebrand, E., Brügmann, G., Von Der Handt, A., Büchl, A. and Hofmann, A.W. (2008) Ancient, highly heterogeneous mantle beneath Gakkel ridge, Arctic Ocean. *Nature* **452**(7185), 311-316.

Liu, J., Riches, A.J.V., Pearson, D.G., Luo, Y., Kienlen, B., Kjarsgaard, B.A., Stachel, T. and Armstrong, J.P. (2016) Age and evolution of the deep continental root beneath the central Rae craton, northern Canada. *Precambrian Res.* **272**, 168-184.

Lorand, J.-P. and Luguet, A. (2016) Chalcophile and siderophile elements in mantle rocks: Trace elements controlled by trace minerals. *Rev. Mineral. Geochem.* **81**, 441-488.

Lorand, J.-P., Luguet, A. and Alard, O. (2013) Platinum-group element systematics and petrogenetic processing of the continental upper mantle: A review. *Lithos* **164**, 2-21.

Luguet, A., Shirey, S.B., Lorand, J.-P., Horan, M.F. and Carlson, R.W. (2007) Residual platinum-group minerals from highly depleted harzburgites of the Lherz massif (France) and their role in HSE fractionation of the mantle. *Geochim. Cosmochim. Acta* **71**, 3082-3097.

Maier, W.D., Peltonen, P., McDonald, I., Barnes, S., Barnes, S.-J., Hatton, C. and Viljoen, F. (2012) The concentration of platinum-group elements and gold in southern African and Karelian kimberlite-hosted mantle xenoliths: Implications for the noble metal content of the Earth's mantle. *Chem. Geol.* **302**, 119-135.

McKenzie, D. and Priestley, K. (2016). Speculations on the formation of cratons and cratonic basins. *Earth Planet. Sci. Lett.* **435**, 94-104.

Meisel, T., Walker, R.J., Irving, A.J. and Lorand, J.-P. (2001) Osmium isotopic compositions of mantle xenoliths: a global perspective. *Geochim. Cosmochim. Acta* **65**, 1311-1323.

Meisel, T., and Moser, J. (2004) Reference materials for geochemical PGE analysis: new analytical data for Ru, Rh, Pd, Os, Ir, Pt and Re by isotope dilution ICP-MS in 11 geological reference materials. *Chemical Geology* **208**(1), 319-338.

Meisel, T., Reisberg, L., Moser, J., Carignan, J., Melcher, F. and Brügmann, G. (2003) Re–Os systematics of UB-N, a serpentinized peridotite reference material. *Chem. Geol.* **201**, 161-179.

Millonig, L., Zeh, A., Gerdes, A. and Klemd, R. (2008) Neoarchaean high-grade metamorphism in the Central Zone of the Limpopo Belt (South Africa): Combined petrological and geochronological evidence from the Bulai pluton. *Lithos* **103**, 333-351.

Mouri, H., Maier, W. and Brandl, G. (2013) On the possible occurrence of komatiites in the Archaean high-grade polymetamorphic Central Zone of the Limpopo Mobile Belt, South Africa. *S. Afr. J. Geol.* **116**, 55-66.

Mouri, H., Whitehouse, M., Brandl, G. and Rajesh, H. (2009) A magmatic age and four successive metamorphic events recorded in zircons from a single meta-anorthosite sample in the Central Zone of the Limpopo Belt, South Africa. *J. Geol. Soc.* **166**, 827-830.

Nanne, J.A., Millet, M.A., Burton, K.W., Dale, C.W., Nowell, G.M., and Williams, H.M. (2017). High precision osmium stable isotope measurements by double spike MC-ICP-MS and N-TIMS. *Journal of Analytical Atomic Spectrometry* **32**, 749-765.

Palesskii, S.V., Nikolaeva, I.V., Koz'menko, O.A., and Anoshin, G.N. (2009) Determination of platinum-group elements and rhenium in standard geological samples by isotope dilution with mass-spectrometric ending. *Journal of Analytical Chemistry* **64**(3), 272-276.

Parkinson, I.J., Hawkesworth, C.J. and Cohen, A.S. (1998) Ancient mantle in a modern arc: Osmium isotopes in Izu-Bonin-Mariana forearc peridotites. *Science* **281**(5385), 2011-2013.

Pearson, D.G., Carlson, R., Shirey, S., Boyd, F. and Nixon, P. (1995) Stabilisation of Archaean lithospheric mantle: A Re Os isotope study of peridotite xenoliths from the Kaapvaal craton. *Earth Planet. Sci. Lett.* **134**, 341-357.

Pearson, D.G. (1999) The age of continental roots. *Lithos* **48**, 171-194.

Pearson, D.G. and Woodland, S.J. (2000) Solvent extraction/anion exchange separation and determination of PGEs (Os, Ir, Pt, Pd, Ru) and Re–Os isotopes in geological samples by isotope dilution ICP-MS. *Chemical Geology* **165**, 87-107.

Pearson, D., Irvine, G., Carlson, R., Kopylova, M. and Ionov, D. (2002) The development of lithospheric keels beneath the earliest continents: Time constraints using PGE and Re-Os isotope systematics. *Geological Society, London, Special Publications* **199**, 65-90.

Pearson, D., Irvine, G., Ionov, D., Boyd, F. and Dreibus, G. (2004) Re–Os isotope systematics and platinum group element fractionation during mantle melt extraction: a study of massif and xenolith peridotite suites. *Chem. Geol.* **208**, 29-59.

Pearson, D. and Wittig, N. (2008) Formation of Archaean continental lithosphere and its diamonds: the root of the problem. *J. Geol. Soc.* **165**, 895-914.

Pearson, D. and Wittig, N. (2014) The formation and evolution of cratonic mantle lithosphere: Evidence from mantle xenoliths. *Treatise on geochemistry* **2**, 255-292.

Puchtel, I.S., Humayun, M., Campbell, A.J., Sproule, R.A. and Lesher, C.M. (2004) Platinum group element geochemistry of komatiites from the Alexo and Pyke Hill areas, Ontario, Canada. *Geochim. Cosmochim. Acta* **68**(6), 1361-1383.

Reisberg, L. and Lorand, J.P. (1995) Longevity of sub-continental mantle lithosphere from osmium isotope systematics in orogenic peridotite massifs. *Nature* **376** 159.

Reisberg, L. and Meisel, T. (2002) The Re-Os Isotopic System: A Review of Analytical Techniques. *Geostand. Newslett.* **26**, 249-267.

Reisberg, L., Lorand, J.-P. and Bedini, R.M. (2004) Reliability of Os model ages in pervasively metasomatized continental mantle lithosphere: a case study of Sidamo spinel peridotite xenoliths (East African Rift, Ethiopia). *Chem. Geol.* **208**, 119-140.

Richardson, S., Gurney, J., Erlank, A. and Harris, J. (1984) Origin of diamonds in old enriched mantle. *Nature* **310**, 198-202.

Richardson, S., Pöml, P., Shirey, S. and Harris, J. (2009) Age and origin of peridotitic diamonds from Venetia, Limpopo Belt, Kaapvaal–Zimbabwe craton. *Lithos* **112**, 785-792.

Richardson, S., Shirey, S., Harris, J. and Carlson, R. (2001) Archean subduction recorded by Re–Os isotopes in eclogitic sulfide inclusions in Kimberley diamonds. *Earth Planet. Sci. Lett.* **191**, 257-266.

Richardson, S.H. and Shirey, S.B. (2008) Continental mantle signature of Bushveld magmas and coeval diamonds. *Nature* **453**, 910-913.

Rigby, M., Basson, I., Kramers, J., Gräser, P. and Mavimbela, P. (2011) The structural, metamorphic and temporal evolution of the country rocks surrounding Venetia Mine, Limpopo Belt, South Africa: Evidence for a single palaeoproterozoic tectono-metamorphic event with implications for a tectonic model. *Precambrian Res.* **186**, 51-69.

Rollinson, H. (2010) Coupled evolution of Archean continental crust and subcontinental lithospheric mantle. *Geology* **38**, 1083-1086.

Rudnick, R.L. and Walker, R.J. (2009) Interpreting ages from Re–Os isotopes in peridotites. *Lithos* **112**, 1083-1095.

Shirey, S.B., Harris, J.W., Richardson, S.H., Fouch, M.J., James, D.E., Cartigny, P., Deines, P. and Viljoen, F. (2002) Diamond genesis, seismic structure, and evolution of the Kaapvaal-Zimbabwe craton. *Science* **297**, 1683-1686.

Shirey, S.B. and Walker, R.J. (1998) The Re-Os isotope system in cosmochemistry and high-temperature geochemistry. *Annual Review of Earth and Planetary Sciences* **26**, 423-500.

Simon, N.S., Carlson, R.W., Pearson, D.G. and Davies, G.R. (2007) The origin and evolution of the Kaapvaal cratonic lithospheric mantle. *J. Petrol.* **48**, 589-625.

Simon, N.S., Irvine, G.J., Davies, G.R., Pearson, D.G. and Carlson, R.W. (2003) The origin of garnet and clinopyroxene in "depleted" Kaapvaal peridotites. *Lithos* **71**, 289-322.

Smit, K., Stachel, T., Creaser, R., Ickert, R., DuFrane, S., Stern, R. and Seller, M. (2014) Origin of eclogite and pyroxenite xenoliths from the Victor kimberlite, Canada, and implications for Superior craton formation. *Geochim. Cosmochim. Acta* **125**, 308-337.

Smoliar, M.I., Walker, R.J. and Morgan, J.W. (1996) Re-Os ages of group IIA, IIIA, IVA, and IVB iron meteorites. *Science* **271**, 1099.

Snow, J.E., and Reisberg, L. (1995) Os isotopic systematics of the MORB mantle: results from altered abyssal peridotites. *Earth Planet. Sci. Lett.* **133**(3-4), 411-421.

Stiefenhofer, J., Viljoen, K., Tainton, K., Dobbe, R. and Hannweg, G. (1999) The petrology of a mantle xenolith suite from Venetia, South Africa, in: Gurney, J., Gurney, J., Pascoe, M., Richardson, S. (Eds.), Proceedings of the VIIth International Kimberlite Conference, 836-845.

Taylor, W.R. (1998). An experimental test of some geothermometer and geobaro-meter formulations for upper mantle peridotites with application to the ther-mobarometry of fertile lherzolite and garnet websterite. *Neues Jahrbuch für Mineralogie-Abhandlungen*, 381-408.

van Acken, D., Becker, H., Walker, R.J., McDonough, W.F., Wombacher, F., Ash, R.D. and Piccoli, P.M. (2010). Formation of pyroxenite layers in the Totalp ultramafic massif (Swiss Alps)–insights from highly siderophile elements and Os isotopes. *Geochim. Cosmochim. Acta* **74**, 661-683.

van der Meer, Q.H.A., Klaver, M., Waight, T.E. and Davies, G.R. (2013) The provenance of sub-cratonic mantle beneath the Limpopo Mobile Belt (South Africa). *Lithos* **170**, 90-104.

Völkening, J., Walczyk, T. and Heumann, K.G. (1991) Osmium isotope ratio determinations by negative thermal ionization mass spectrometry. *International Journal of Mass Spectrometry and Ion Processes* **105**, 147-159.

Wainwright, A.N., Luguet, A., Fonseca, R.O.C. and Pearson, D.G. (2015) Investigating metasomatic effects on the ^{187}Os isotopic signature: A case study on micrometric base metal sulphides in metasomatised peridotite from the Letlhakane kimberlite (Botswana). *Lithos* **232**, 35-48.

Wainwright, A.N., Luguet, A., Schreiber, A., Fonseca, R.O.C., Nowell, G.M., Lorand, J.P., Wirth, R. and Janney, P.E. (2016) Nanoscale variations in ^{187}Os isotopic composition and HSE systematics in a Bultfontein peridotite. *Earth Planet. Sci. Lett.* **447**, 60-71.

Walker, R., Carlson, R., Shirey, S. and Boyd, F. (1989) Os, Sr, Nd, and Pb isotope systematics of southern African peridotite xenoliths: implications for the chemical evolution of subcontinental mantle. *Geochim. Cosmochim. Acta* **53**, 1583-1595.

Walker, R. J., Horan, M. F., Morgan, J. W., Becker, H., Grossman, J. N., & Rubin, A. E. (2002). Comparative ^{187}Re-^{187}Os systematics of chondrites: Implications regarding early solar system processes. *Geochimi. Cosmochim. Acta* **66**, 4187-4201.

Walter, M.J. (1998) Melting of garnet peridotite and the origin of komatiite and depleted lithosphere. *J. Petrol.* **39**, 29-60.

Xie, H., Kröner, A., Brandl, G. and Wan, Y. (2017) Two orogenic events separated by 2.6 Ga mafic dykes in the Central Zone, Limpopo Belt, southern Africa. *Precambrian Res.* **289**, 129-141.

Zeh, A., Gerdes, A., Barton, J. and Klemd, R. (2010) U–Th–Pb and Lu–Hf systematics of zircon from TTG's, leucosomes, meta-anorthosites and quartzites of the Limpopo Belt (South Africa): constraints for the formation, recycling and metamorphism of Palaeoarchaean crust. *Precambrian Res.* **179**, 50-68.

Zeh, A., Gerdes, A., Klemd, R. and Barton, J. (2008) U–Pb and Lu–Hf isotope record of detrital zircon grains from the Limpopo Belt–evidence for crustal recycling at the Hadean to early-Archean transition. *Geochim. Cosmochim. Acta* **72**, 5304-5329.

Zeh, A., Gerdes, A., Klemd, R. and Barton, J.M. (2007) Archaean to Proterozoic crustal evolution in the central zone of the Limpopo Belt (South Africa–Botswana): constraints from combined U–Pb and Lu–Hf isotope analyses of zircon. *J. Petrol.* **48**, 1605-1639.

Table 1. *Whole rock Re and Os concentrations and isotope compositions, Re-Os analyses with V sample number are from Carlson et al. (1999). HT: high-temperature, TL: low-temperature, hz: harzburgite, lhz: lherzolite, pyr: pyroxenite, Ref.: reference standard. Al_2O_3 concentrations and Mg# in olivine are from van der Meer et al. (2013), Stiefenhofer et al. (1999) and Carlson et al. (1999), n.r.: no report of data available, n/a: calculation not applicable. Chondritic mantle parameters ($^{187}Os/^{188}Os = 0.1283$ and $^{187}Re/^{188}Os = 0.422$) for the calculation of γOs and model ages are from Walker et al. (2002). Kimberlite-corrected Re-intercept $Re_{(int)}$ concentrations for groups I, II and III are calculated at the intercept with the 3.28 Ma "isochron", also see Fig. 5a. Pressure and*

*Temperature are calculated iteratively using the garnet-orthopyroxene P_{NG85} barometer of Nickel and Green (1985) and the garnet-orthopyroxene T_{NG09} thermometer after Nimis and Grütter (2010), clinopyroxene-bearing lithologies were compared to the Taylor (1998) 2-pyroxene thermometer for validation (not reported). Exceptions are a: where $T_{[Ca\text{-}OPX09]}$ thermometry (Nimis and Grütter 2010) was used for garnet-free samples to calculate P at the crossing with the Venetian "steady-state geotherm" (van der Meer et al., 2013), b: garnet and pyroxene are in major element disequilibrium, c: mineral data is lacking or d: the lithology is unsuitable for conventional P-T calculation. Depth calculation assumes 50 km of crust with a pressure of 1.5 GPa at the base and a uniform average lithospheric mantle density of 3.5 g*cm^{-3}. Replicate analyses are shown in italic with analyses conducted in Durham designated by "(D)". The measured $^{187}Os/^{188}Os$ isotopic composition of GP-13 ($^{187}Os/^{188}Os$ = 0.1260 ± 0.0002, 2SE) is within uncertainty of published values, the Durham average (n = 35, $^{187}Os/^{188}Os$ = 0.1261 ± 0.0005, 2σ), and average determined at the University of Alberta (n = 4, $^{187}Os/^{188}Os$ = 0.1262 ± 0.0010, 2σ). However, the corrected value included in the data table has a $^{187}Os/^{188}Os$ composition that is resolvable and lower than has been reported previously for distinct powder aliquots of this in-house peridotite reference material. This variation may reflect; 1) real difference between the Os-isotopic composition of the measured powder fraction and those studied previously ['nugget effect'], or 2) an over-correction based on the average total procedural blank composition.*

Table 2. *Platinum group element concentrations for selected samples. Os concentrations from the same sample solution and also reported with duplicate isotope analyses in table 1. With the exception of Pt, the PGE-abundances of GP-13 are within uncertainty of values reported in previous studies (e.g., Meisel and Moser, 2004; Puchtel et al., 2004; Palesskii et al., 2009)*

Figure 1. *Map of the Kalahari Craton and subdivision between the separate terranes, including the Limpopo Mobile Belt and its zones, modified from van der Meer et al. (2013), after de Wit et al. (1992). Outcrop of the 2.05 Ga Bushveld LIP is shown in black. Dashed lines indicate national boundaries. SA, South Africa; NAM, Namibia; LS, Lesotho; SW, Swaziland; BW, Botswana; ZIM, Zimbabwe.*

Figure 2. *Plots of Re vs. Os abundances (a) and Re/Os vs. Al_2O_3 content (b) for the Venetia xenolith suite, including data from Carlson et al. (1999). In (a), samples are divided into five colour-coded groups (Roman capitals) according to their Re and Os contents and $^{187}Os/^{188}Os$ systematics. Generalised descriptions are as follows: group I samples have Re/Os between 0.04 and 0.01, group II samples have higher Re/Os at similar Os content, group III have higher Re/Os at lower Os content, group IV have low Re/Os at similar Os content; group V samples are characterised by highly disturbed $^{187}Os/^{188}Os$ and cannot be distinguished on the basis of Re and Os contents alone. See text for further discussion. In (b), the Venetia samples largely overlap with the field for other Kalahari Craton mantle xenoliths. Pyroxenite AT 1198, at 8.17 wt.% Al_2O_3 and Re/Os = 7.3, falls off scale. The mantle melting trends at pressures of 3, 5 and 7 GPa (all at ΔFMQ-2) and the field for Kalahari mantle xenoliths are from Aulbach et al. (2016); whole rock Al_2O_3 data are from Carlson et al. (1999) and van der Meer et al. (2013).*

Figure 3. *$^{187}Os/^{188}Os$ vs. $^{187}Re/^{188}Os$ isochron diagram for the Venetia xenolith suite; symbols indicate lithology whereas colours refer to the groups based on Re-Os systematics. Group I samples cluster around a 3.28 Ga isochron; this reference line is based on the average T_{MA} of the group I samples and is not a regression in this diagram. Group II samples are displaced away from group I along a 533 Ma vector, consistent with Re addition during kimberlite eruption. Group III samples (AT1324 and AT1338) are characterised by very low Os contents and fall on a 533 Ma (kimberlite eruption age) reference line originating from the isochron initial ratio. Group IV samples have $^{187}Os/^{188}Os$ values ranging from 0.10948 to 11930, but all have low $^{187}Re/^{188}Os$ (≤0.02). See text for further discussion. The inset shows garnet clinopyroxenite AT 1198, which has high $^{187}Re/^{188}Os$ and a radiogenic Os isotope composition. A tie line with CHUR yields a (T_{MA}) age of 2.62 Ga. Chondritic mantle after Walker et al. (2002).*

Figure 4. *Platinum group element concentrations of selected samples. A: Platinum group elements normalised to Primitive Upper Mantle (PUM) after Becker et al. (2006). Compatible I-PGE (Os, Ir, Ru) have higher relative concentrations than P-PGE (Pt, Pd) and Re except for Ru in low I-PGE sample ATC 725. B: PUM normalised Pt/Ir versus Os/Ir illustrates correlations corresponding to melt depletion trends and the lack of noticeable oxidative Os loss related to weathering (e.g. Handler et al., 1999).*

Figure 5. *Re and Os concentration systematics in the group I and II samples. a) shows how "isochron intercept" $^{187}Re/^{188}Os$, and thus Re/Os and Re content, are calculated. This assumes that all excess Re that causes the samples to fall off the 3.28 Ga mean T_{MA} age reference line is added during kimberlite magmatism at 533 Ma, and that Os contents remained unchanged. In b) and c), systematic variation of "isochron intercept" Re and Re/Os with Os suggests that the Re-Os budget is controlled by two components, as discussed in the text. A correlation between measured Re and Os is also observed in the group I samples if no corrections are applied. Samples are colour coded for olivine Mg# as proxy for degree of depletion. Samples with lowest olivine Mg# have homogeneous Os contents consistent with the melt depletion trend whereas samples with higher olivine Mg# show a considerably wider variation. An approximated fractional melting column model for an Archaean Convecting Mantle (ACM) source (5 GPa, ΔFMQ -2) with increments of 1.1% where 1% of the melt is added to the starting composition of the following increment in c) is taken from Aulbach et al. (2016). The dashed lines represent mixing between the two hypothetical Os-bearing components A and B that control the Re and Os budged of the peridotites.*

Figure 6. *Variation of $^{187}Os/^{188}Os_{EA}$ for group I, II and III samples with indices of melt depletion. Sample ATC 747 ($^{187}Os/^{188}Os_{EA}$ = 0.1166) is excluded from b) for scaling purposes. PUM PGE normalisation values are from Becker et al. (2006). Range of Os contents in fertile and depleted Archaean mantle in d) is from Aulbach et al. (2016).*

Figure 7. *Variation of Re-Os systematics with modal orthopyroxene content of the group I and II samples. a) The Venetia xenoliths show no correlation between $^{187}Os/^{188}Os_{EA}$ and modal orthopyroxene content, in contrast to*

Kimberley (Kaapvaal Craton) xenoliths; data from (Simon et al., 2007). b) Re/Os versus Os content, symbols identical to Figure 5c but with samples colour coded for modal orthopyroxene content.

Figure 8. *Schematic model for the Re-Os evolution of the Venetia xenolith suite during SCLM stabilisation. Melting at 3.35 Ga produces thick mafic crust and a complementary refractory mantle that records 20-30 % melt depletion, as illustrated by the "low olivine Mg# samples". Melt model in A is the same as in Figure 5. Residue compositions have decreasing Re/Os with increasing melt extraction, auto-refertilisation can cause minor elevation of Re/Os and retain some Re in the residue. B: Rapid recycling of mafic crust at 3.28 Ga causes reaction of the refractory mantle with percolating melts, stimulating an additional 10-15 % melting and formation of aluminous orthopyroxene. Remobilisation of component B leaves some samples relatively depleted in Os and others enriched. As component B controls the Re budget, Re/Os is only mildly affected by remobilisation except at low Os concentrations (<200 ppb).*

Figure 9. *Distribution of T_{MA} and T_{RD} model ages for the Venetia xenoliths (excluding group V). Group I samples display T_{MA} ages that reflect timing of melt extraction and lithosphere stabilisation, whereas the group II samples yield fictitious T_{MA} ages due to recent Re addition. Rhenium-depletion ages (T_{RD}) are the same for both sample groups, but do not have any geological significance and the overlap with the Kaapvaal-Limpopo collision age is merely coincidental. Only group III samples that lost Re and most of their Os during SCLM stabilisation yield meaningful T_{RD} ages.*

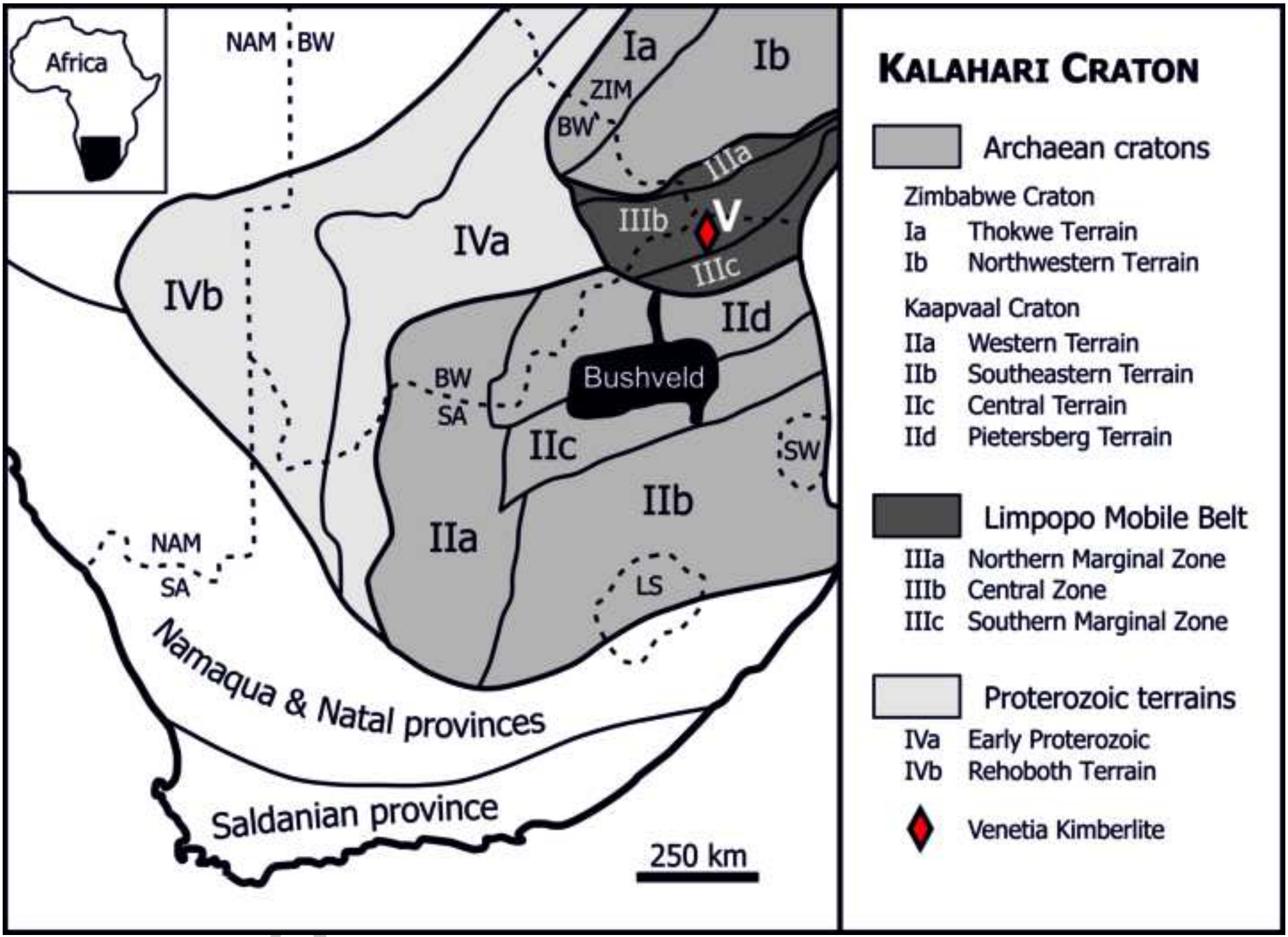

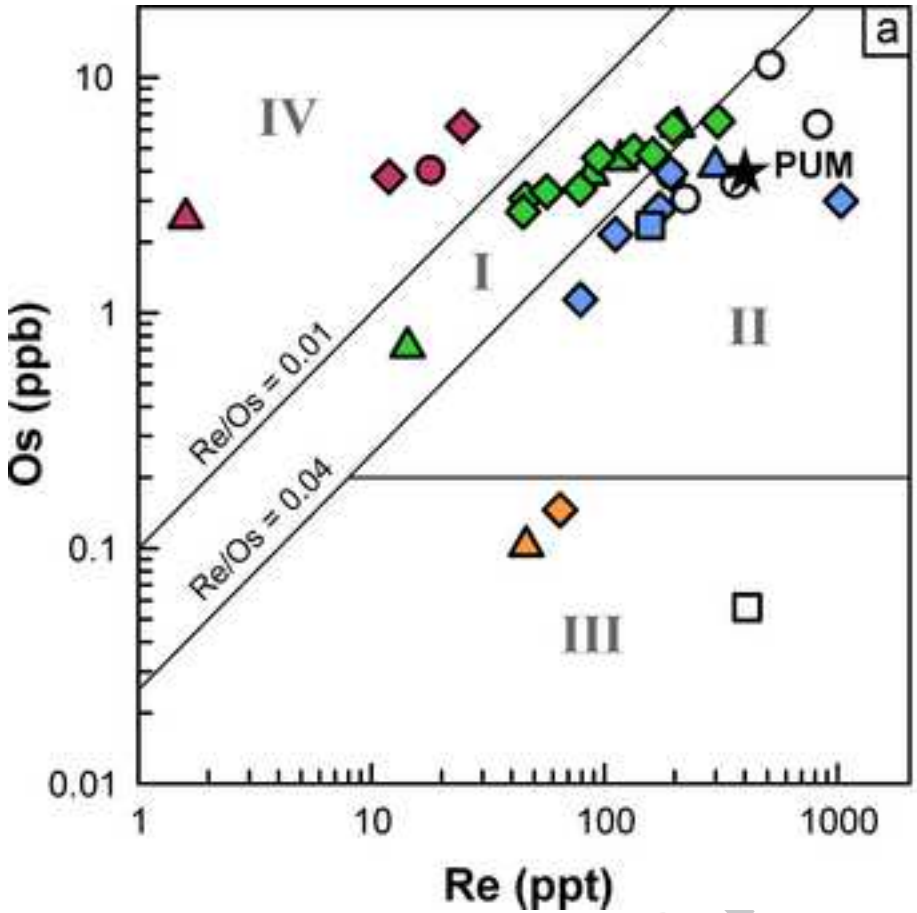

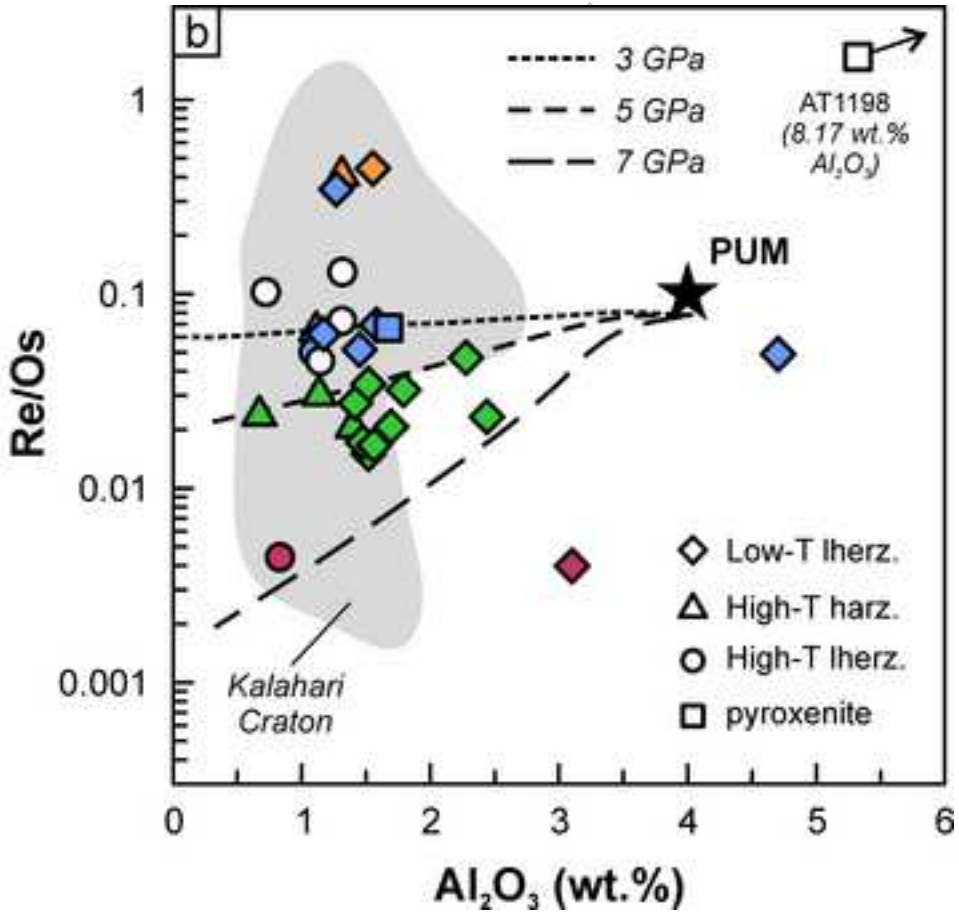

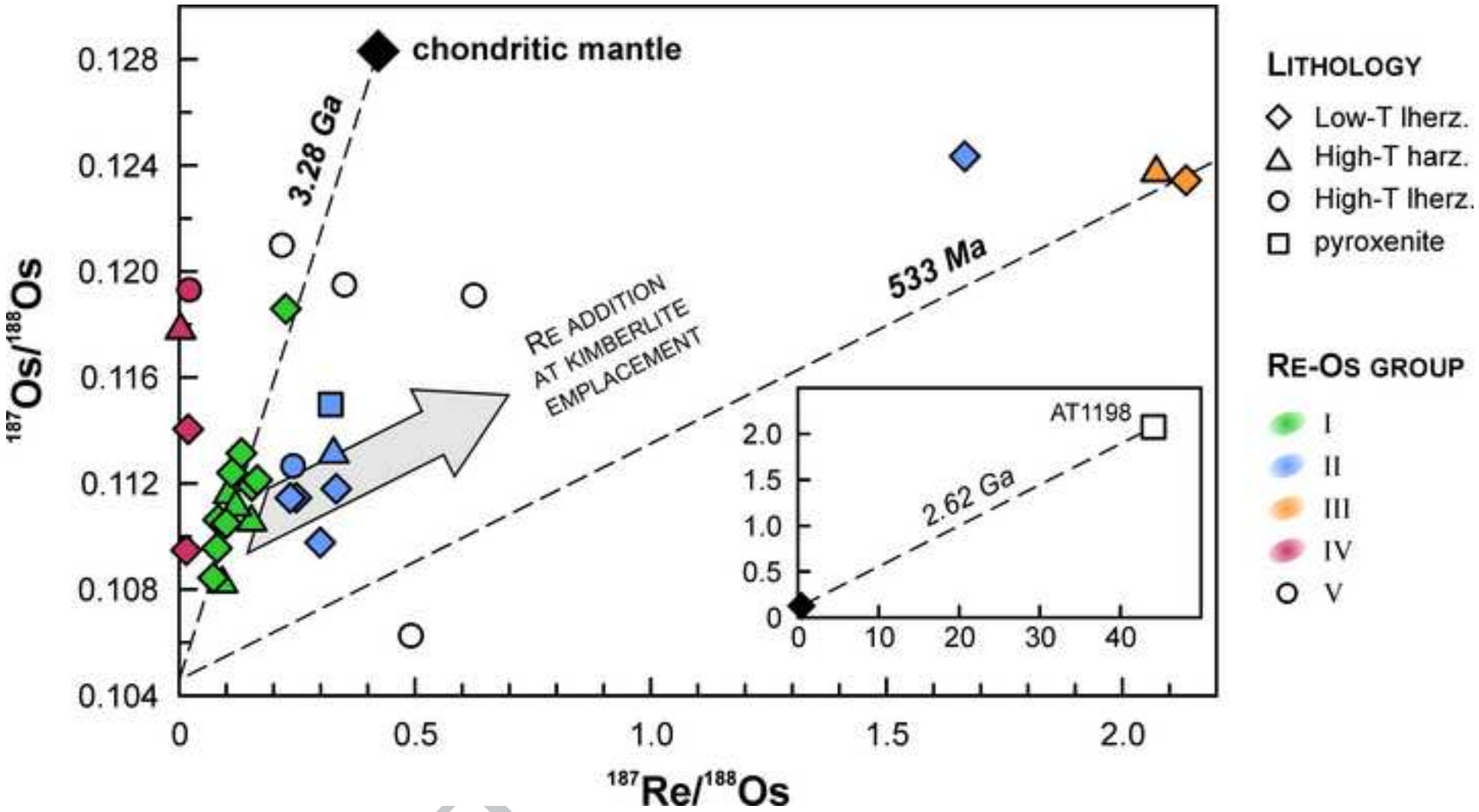

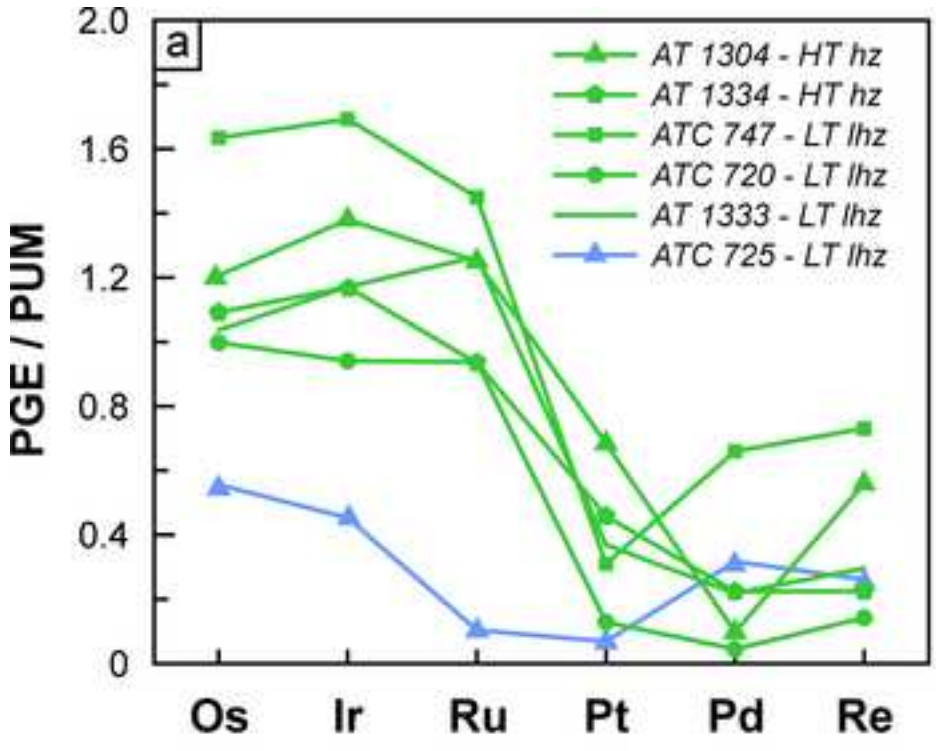

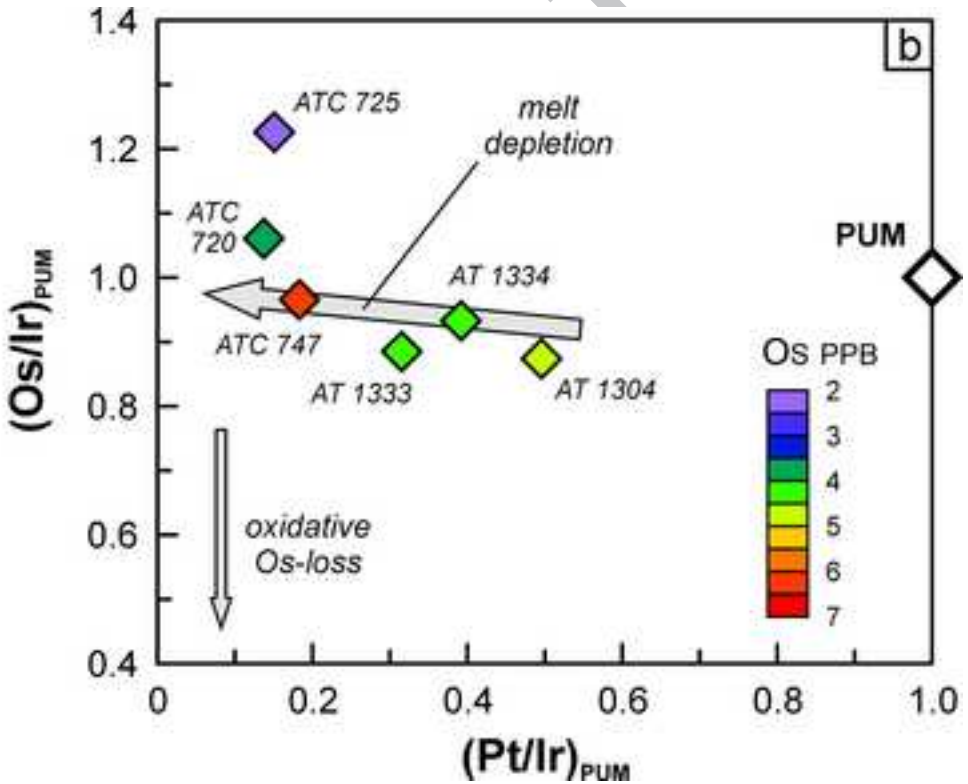

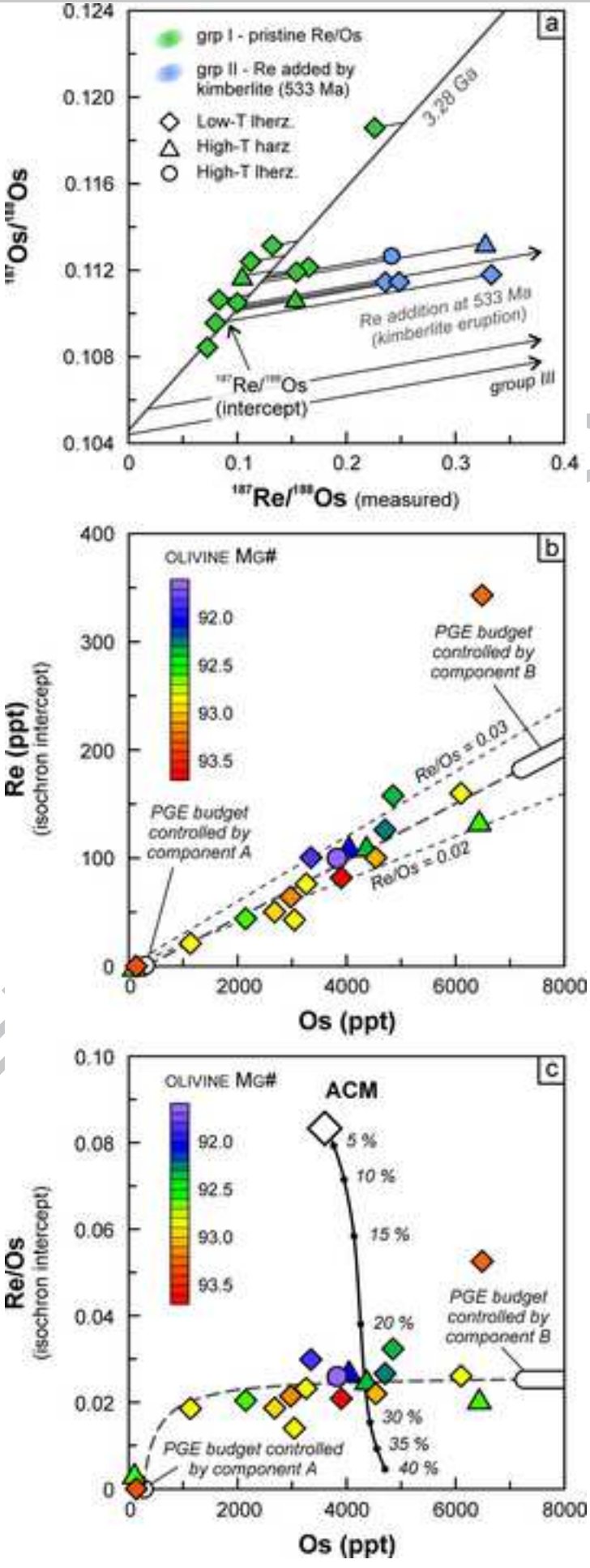

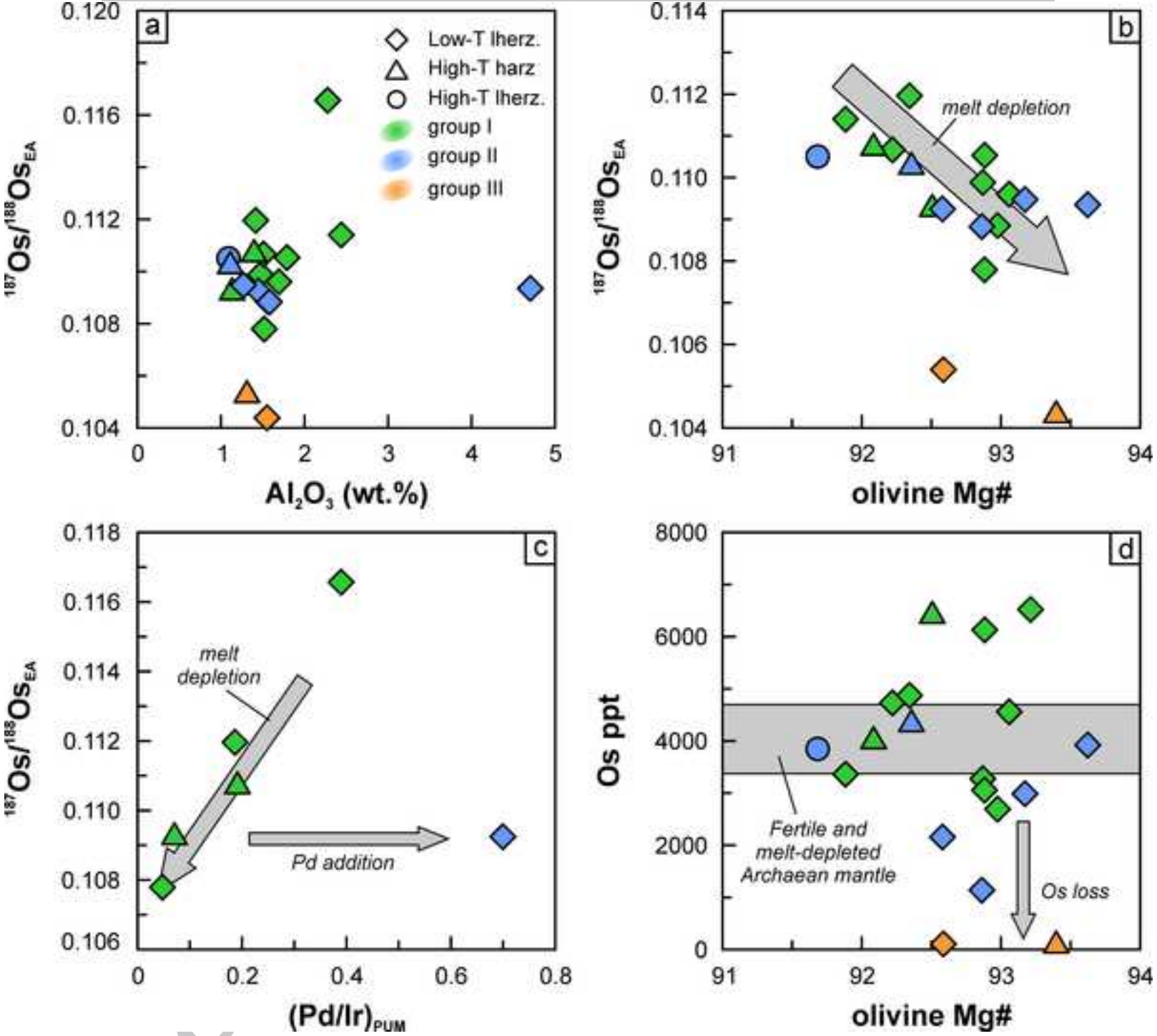

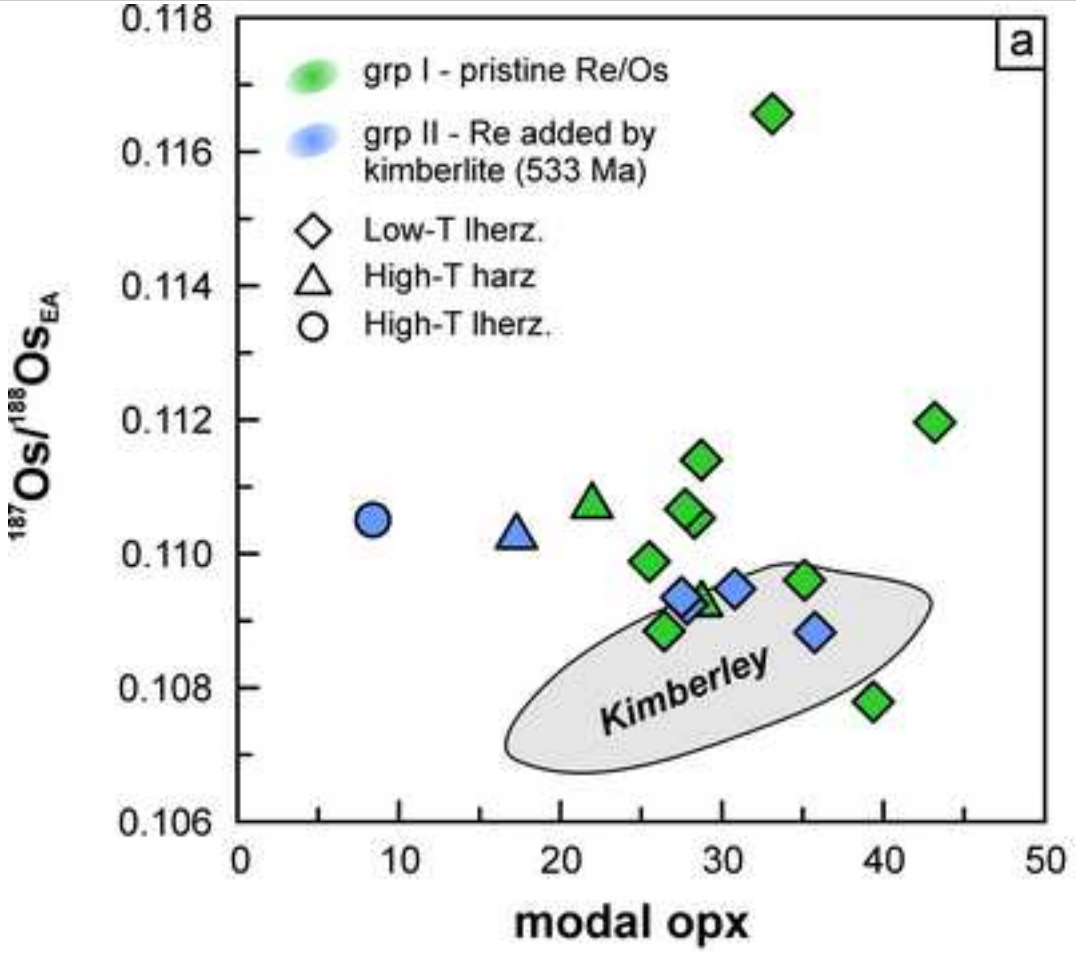

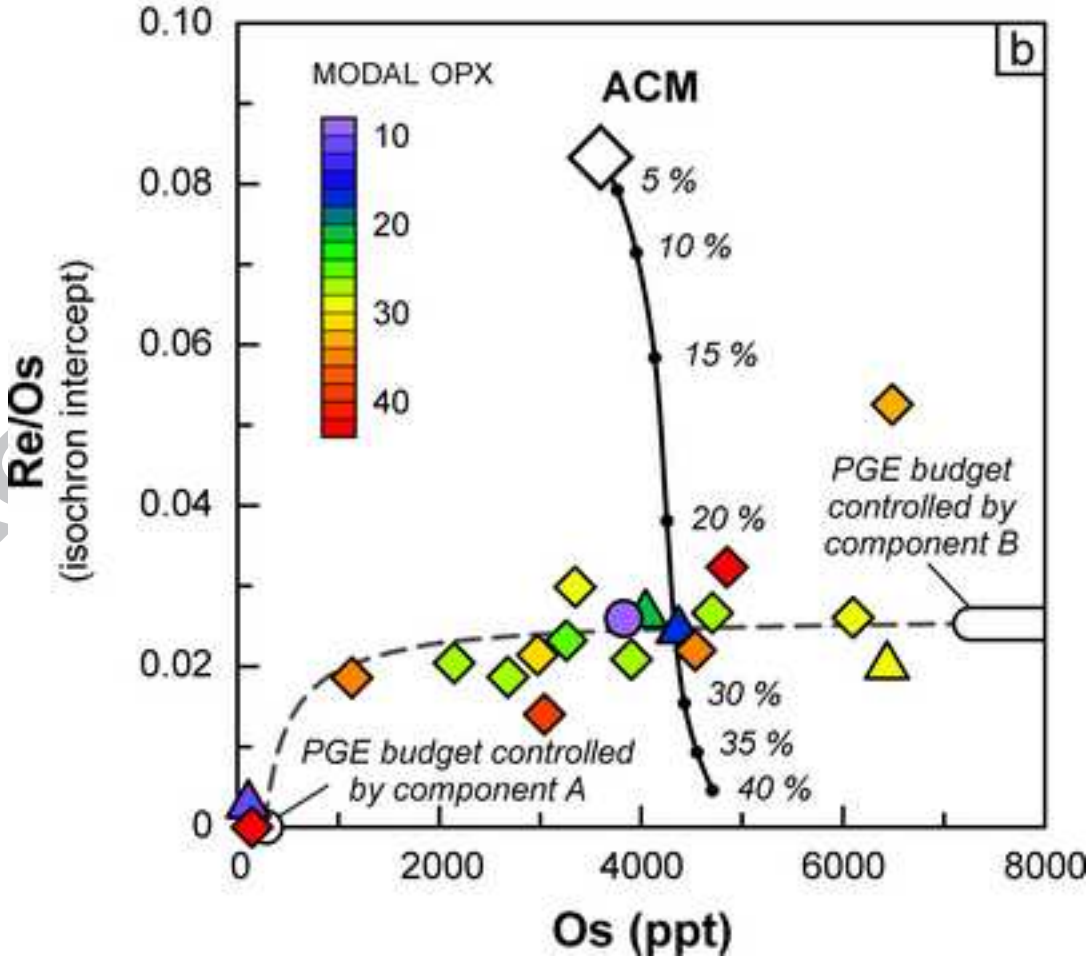

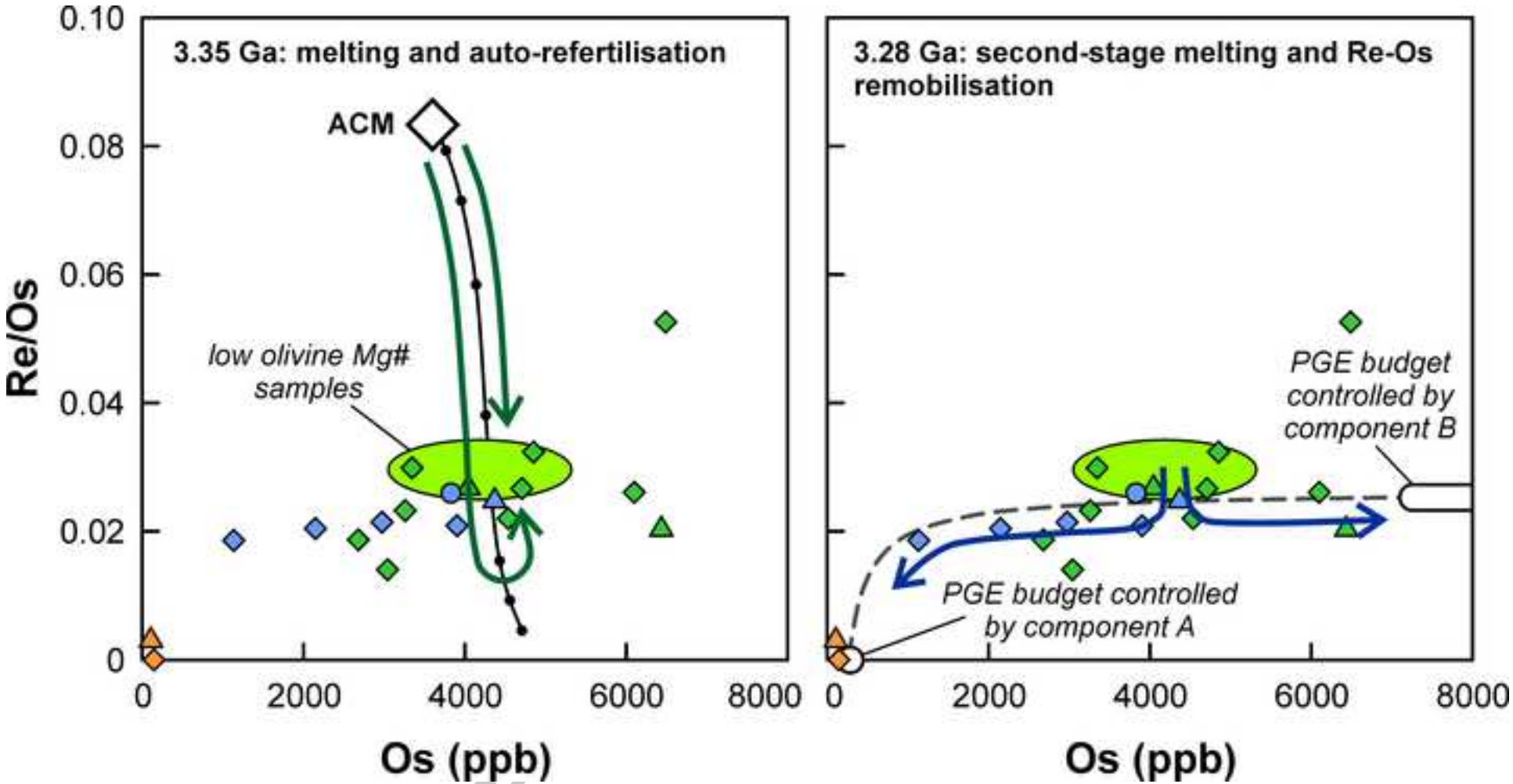

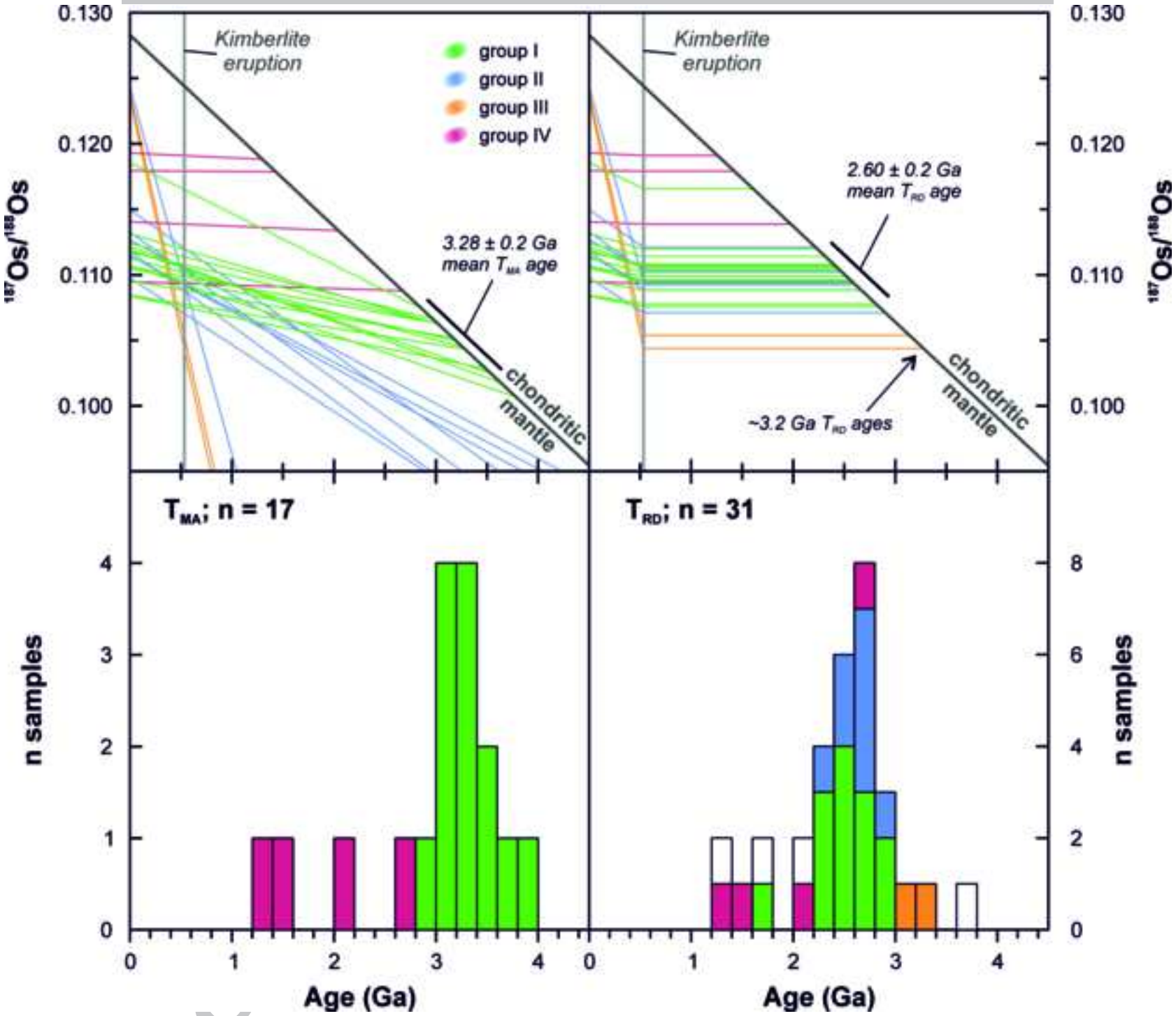

Table 1. *Whole rock Re and Os concentrations and isotope compositions, Re-Os analyses with V sample number are from Carlson et al. (1999). HT: high-temperature, TL: low-temperature, hz: harzburgite, lhz: lherzolite, pyr: pyroxenite, Ref.: reference standard. Al_2O_3 concentrations and Mg# in olivine are from van der Meer et al. (2013), Stiefenhofer et al. (1999) and Carlson et al. (1999), n.r.: no report of data available, n/a: calculation not applicable. Chondritic mantle parameters ($^{187}Os/^{188}Os$ = 0.1283 and $^{187}Re/^{188}Os$ = 0.422) for the calculation of γOs and model ages are from Walker et al. (2002). Kimberlite-corrected Re-intercept $Re_{(int)}$ concentrations for groups I, II and III are calculated at the intercept with the 3.28 Ma "isochron", also see Fig. 5a. Pressure and Temperature are calculated iteratively using the garnet-orthopyroxene P_{NG85} barometer of Nickel and Green (1985) and the garnet-orthopyroxene T_{NG09} thermometer after Nimis and Grütter (2010), clinopyroxene-bearing lithologies were compared to the Taylor (1998) 2-pyroxene thermometer for validation (not reported). Exceptions are a: where $T_{[Ca\text{-}OPX09]}$ thermometry (Nimis and Grütter 2010) was used for garnet-free samples to calculate P at the crossing with the Venetian "steady-state geotherm" (van der Meer et al., 2013), b: garnet and pyroxene are in major element disequilibrium, c: mineral data is lacking or d: the lithology is unsuitable for conventional P-T calculation. Depth calculation assumes 50 km of crust with a pressure of 1.5 GPa at the base and a uniform average lithospheric mantle density of 3.5 g*cm^{-3}. Replicate analyses are shown in italic with analyses conducted in Durham designated by "(D)". The measured $^{187}Os/^{188}Os$ isotopic composition of GP-13 ($^{187}Os/^{188}Os$ = 0.1260 ± 0.0002, 2SE) is within uncertainty of published values, the Durham average (n = 35, $^{187}Os/^{188}Os$ = 0.1261 ± 0.0005, 2σ), and average determined at the University of Alberta (n = 4, $^{187}Os/^{188}Os$ = 0.1262 ± 0.0010, 2σ). However, the corrected value included in the data table has a $^{187}Os/^{188}Os$ composition that is resolvable and lower than has been reported previously for distinct powder aliquots of this in-house peridotite reference material. This variation may reflect; 1) real difference between the Os-isotopic composition of the measured powder fraction and those studied previously ['nugget effect'], or 2) an over-correction based on the average total procedural blank composition.*

group	type	sample	WR Al_2O_3	Ol Mg#	Re	Os	Re/Os	$Re_{(int)}$	$^{187}Os/^{188}Os$	2 SE	γOs	$^{187}Re/^{188}Os$	2 SE	$^{187}Os/^{188}Os_{EA}$	T_{MA}	T_{RD}	T_{NG09}	P_{NG85}	Depth
			wt.%		ppt	ppb		ppt						533 Ma	Ga	Ga	°C	GPa	km
1	HT hz	AT 1304	1.14	92.5	206	6.47	0.032	135	0.11070	0.00003	-13.7	0.1533	0.0008	0.1093	3.81	2.64	1337	5.6	167
	HT hz	*AT-1304 (D)*			*196*	*4.70*	*0.042*		*0.11085*	*0.00012*	*-13.6*	*0.2001*	*0.0020*	*0.1091*	*4.54*	*2.68*			
1	LT lhz	AT 1333	1.42	92.3	134	4.88	0.027	158	0.11314	0.00008	-11.8	0.1320	0.0007	0.1120	3.06	2.28	808	2.8	87
	LT lhz	*AT-1333 (D)*			*115*	*4.18*	*0.028*		*0.11346*	*0.00028*	*-11.6*	*0.1326*	*0.0013*	*0.1123*	*3.00*	*2.24*			
	LT lhz	*AT-1333 (D)*			*106*	*4.27*	*0.025*		*0.11431*	*0.00024*	*-10.9*	*0.1200*	*0.0012*	*0.1132*	*2.72*	*2.10*			

	LT lhz	*AT-1333 (D)*			*89*	*3.68*	*0.024*		*0.11292*	*0.00011*	*-12.0*	*0.1160*	*0.0012*	*0.1119*	*2.94*	*2.29*			
1	HT hz	AT 1334	1.40	92.1	88.3	4.06	0.022	111	0.11173	0.00006	-12.9	0.1045	0.0005	0.1108	3.05	2.44	1351	5.5	164
	HT hz	*AT-1334 (D)*			*79*	*4.26*	*0.018*		*0.11085*	*0.00012*	*-13.8*	*0.0887*	*0.0009*	*0.1098*	*3.11*	*2.57*			
1	LT lhz	ATC 720	1.52	92.9	46.0	3.06	0.015	43	0.10844	0.00004	-15.5	0.0724	0.0004	0.1078	3.32	2.85	866	3.3	102
	LT lhz	*ATC 720*			*47*	*3.05*	*0.015*		*0.10825*	*0.00013*	*-15.6*	*0.0740*	*0.0007*	*0.1076*	*3.36*	*2.88*			
	LT lhz	*ATC-720 (D)*			*50*	*3.89*	*0.013*		*0.10766*	*0.00012*	*-16.1*	*0.0616*	*0.0006*	*0.1071*	*3.34*	*2.94*			
1	LT lhz	ATC 722	1.47	92.9	56.5	3.28	0.017	76	0.11062	0.00005	-13.8	0.0830	0.0004	0.1099	3.05	2.56	748	2.2	71
	LT lhz	*ATC 722*			*54*	*3.12*	*0.017*		*0.11068*	*0.00013*	*-13.7*	*0.0835*	*0.0008*	*0.1099*	*3.05*	*2.56*			
1	LT lhz	ATC 724	1.69	93.1	94.7	4.56	0.021	100	0.11050	0.00004	-13.9	0.0999	0.0005	0.1096	3.23	2.60	701	1.8	60
1	LT lhz	ATC 726	1.56	93.0	44.8	2.69	0.017	50	0.10956	0.00007	-14.6	0.0800	0.0004	0.1088	3.20	2.70	811	2.8	87
1	LT lhz	ATC 740	1.79	92.9	196	6.13	0.032	160	0.11191	0.00005	-12.8	0.1541	0.0008	0.1105	3.57	2.48	823	2.9	89
1	LT lhz	ATC 742	1.51	92.2	162	4.73	0.034	126	0.11214	0.00008	-11.7	0.1652	0.0041	0.1107	3.66	2.39	898	3.7	113
1	LT lhz	ATC 747	2.28	93.2	306	6.52	0.047	343	0.11858	0.00005	-7.6	0.2260	0.0011	0.1166	2.91	1.65	796	2.7	83
	LT lhz	*ATC-747 (D)*			*256*	*6.38*	*0.040*		*0.11799*	*0.00010*	*-8.0*	*0.1931*	*0.0019*	*0.1163*	*2.64*	*1.69*			
1	LT lhz	ATC 752	2.44	91.9	78.4	3.36	0.023	100	0.11240	0.00003	-12.4	0.1122	0.0006	0.1114	3.00	2.36	736	2.2	69
1	HT hz	V39	0.67	n.r.	117	4.67	0.025		0.11127	0.00010	-13.3	0.1205	0.0006	0.1102	3.30	2.52	1277	5.1	152
1	HT hz	V86	n.r.	n.r.	14.3	0.750	0.019		0.10837	0.00018	-15.5	0.0917	0.0005	0.1076	3.52	2.88	n/a	n/a	n/a
2	HT hz	AT 1305	1.11	92.4	299	4.39	0.068	111	0.11327	0.00006	-11.7	0.3276	0.0016	0.1103	n/a	2.50	1367	5.4	163
2	LT lhz	AT 1348	1.58	92.9	78.9	1.14	0.069	21	0.11180	0.00016	-12.9	0.3330	0.0017	0.1088	n/a	2.71	831	3.0	92
2	HT lhz	AT 1355	1.09	91.7	193	3.85	0.050	100	0.11266	0.00005	-12.2	0.2415	0.0012	0.1105	n/a	2.48	1395	5.1	153

2	LT lhz	ATC 725	1.45	92.6	112	2.16	0.052	82	0.11146	0.00005	-13.1	0.2485	0.0012	0.1092	n/a	2.65	680	1.7	54
	LT lhz	*ATC-725 (D)*			*91*	*2.17*	*0.042*		*0.11010*	*0.00016*	*-14.2*	*0.2028*	*0.0020*	*0.1083*	*4.79*	*2.78*			
2	pyr	ATC 727	1.68	89.5	157	2.35	0.067	78	0.11497	0.00018	-10.4	0.3214	0.0016	0.1121	n/a	2.26	899	3.6	111
2	LT lhz	ATC 731	1.27	93.2	1033	2.99	0.346	64	0.12434	0.00014	-3.1	1.6661	0.0083	0.1095	n/a	2.62	732	2.2	69
2	LT lhz	ATC 745	4.70	93.6	192	3.92	0.049	82	0.11145	0.00006	-13.1	0.2357	0.0012	0.1094	n/a	2.64	792	2.5	78
2	LT lhz	V73	1.17	n.r.	172	2.77	0.062		0.10977	0.00005	-14.4	0.2991	0.0015	0.1071	n/a	2.94	718	1.9	61
3	LT lhz	AT 1324	1.55	93.4	65	0.15	0.443	0	0.12343	0.00037	-3.8	2.1352	0.0107	0.1044	n/a	3.31	831	3.1	95
3	HT hz	AT 1338	1.31	92.6	46	0.11	0.430	0	0.12388	0.00034	-3.4	2.0722	0.0104	0.1054	n/a	3.17	1155	5.0	149
4	LT lhz	ATC 753	3.10	92.0	24.7	6.20	0.004		0.11404	0.00005	-11.1	0.0191	0.0001	0.1139	2.09	2.02	791	2.5	79
4	HT hz	V32	n.r.	92.7	1.60	2.65	0.001		0.11794	0.00014	-8.1	0.0029	0.0000	0.1179	1.47	1.46	1348	5.8	172
4	LT lhz	V53	n.r.	n.r.	11.9	3.79	0.003		0.10948	0.00008	-14.7	0.0151	0.0001	0.1093	2.71	2.64	n/a	n/a	n/a
4	HT lhz	V61	0.83	n.r.	17.9	4.05	0.004		0.11930	0.00010	-7.0	0.0213	0.0001	0.1191	1.33	1.29	n/a	n/a	n/a
5	HT lhz	AT 1311	1.32	n.r.	821	6.33	0.130		0.11909	0.00027	-7.2	0.6249	0.0031	0.1135	n/a	2.07	n/a	n/a	n/a
5	HT lhz	AT 1315	1.31	90.0	222	3.06	0.073		0.11949	0.00012	-6.9	0.3502	0.0018	0.1164	n/a	1.67	n/a	n/a	n/a
5	HT lhz	AT 1361	1.14	91.6	512	11.33	0.045		0.12098	0.00007	-5.7	0.2177	0.0011	0.1190	2.11	1.30	1278	4.5	136
5	HT lhz	V63	0.72	91.4	363	3.55	0.102		0.10626	0.00009	-17.2	0.4914	0.0025	0.1019	n/a	3.65	1112	5.0	151
	pyr	AT 1198	8.17	n/a	409	0.056	7.299		2.074	0.00189	1516.6	44.11	0.2205	1.681	2.62	n/a	n/a	n/a	n/a
	Ref.	GP-13 (D)			272	3.70	0.073		0.12458	0.00025		0.3540	0.0035	0.12458					

Table 2. *Platinum group element concentrations for selected samples. Os concentrations from the same sample solution and also reported with duplicate isotope analyses in table 1. With the exception of Pt, the PGE-abundances of GP-13 are within uncertainty of values reported in previous studies (e.g., Meisel and Moser, 2004; Puchtel et al., 2004; Palesskii et al., 2009)*

group	type	sample	Re (ppb)	Blk Corr.	Ir (ppb)	Blk Corr.	Pt (ppb)	Blk Corr.	Pd (ppb)	Blk Corr.	Ru (ppb)	Blk Corr.	Os (ppb)	Blk Corr.
2	LT lhz	ATC-725	0.091	4.2%	1.59	0.07%	0.52	9.1%	2.25	0.9%	0.73	8.2%	2.17	0.22%
1	LT lhz	ATC-720	0.050	7.5%	3.29	0.03%	0.98	5.0%	0.32	5.9%	6.56	1.0%	3.89	0.12%
1	HT hz	AT-1334	0.079	4.9%	4.10	0.03%	3.49	1.5%	1.59	1.2%	6.54	1.0%	4.26	0.11%
1	HT hz	AT-1304	0.20	2.0%	4.83	0.02%	5.20	1.0%	0.69	2.8%	8.76	0.7%	4.70	0.10%
1	LT lhz	ATC-747	0.26	1.6%	5.93	0.02%	2.36	0.6%	4.69	0.4%	10.1	0.6%	6.38	0.07%
1	LT lhz	AT-1333	0.12	3.4%	4.13	0.03%	3.71	1.4%	1.69	1.2%	9.14	0.7%	4.18	0.11%
1	LT lhz	AT-1333	0.11	3.6%	4.52	0.02%	2.36	1.4%	1.53	1.3%	6.98	0.9%	4.27	0.11%
1	LT lhz	AT-1333	0.09	3.6%	3.66	0.02%	2.36	1.3%	1.43	1.1%	10.4	0.5%	3.68	0.10%
	LT lhz	AT-1333 av.	0.10		4.1		2.81		1.55		8.86		4.04	
		GP-13 (ref.)	0.27	1.4%	3.52	0.03%	2.36	0.7%	4.89	0.4%	5.92	1.0%	3.70	0.97%